



# *The landscape model: a model for exploring trade-offs between agricultural production and the environment*

Article

Accepted Version

Creative Commons: Attribution-Noncommercial-No Derivative Works 4.0

Coleman, K., Muhammed, S. E., Milne, A. E., Todman, L. C., Dailey, A. G., Glendining, M. J. and Whitmore, A. P. (2017) The landscape model: a model for exploring trade-offs between agricultural production and the environment. *Science of the Total Environment*, 609. pp. 1483-1499. ISSN 0048-9697 doi: <https://doi.org/10.1016/j.scitotenv.2017.07.193>  
Available at <http://centaur.reading.ac.uk/74570/>

It is advisable to refer to the publisher's version if you intend to cite from the work. See [Guidance on citing](#).

Published version at: <http://dx.doi.org/10.1016/j.scitotenv.2017.07.193>

To link to this article DOI: <http://dx.doi.org/10.1016/j.scitotenv.2017.07.193>

Publisher: Elsevier

All outputs in CentAUR are protected by Intellectual Property Rights law, including copyright law. Copyright and IPR is retained by the creators or other copyright holders. Terms and conditions for use of this material are defined in the [End User Agreement](#).

[www.reading.ac.uk/centaur](http://www.reading.ac.uk/centaur)

## **CentAUR**

Central Archive at the University of Reading

Reading's research outputs online

1 Journal: Science of the Total Environment

2 The Landscape Model: a model for exploring trade-offs  
3 between agricultural production and the environment.

4

5 Kevin Coleman<sup>a\*</sup>, Shibu E. Muhammed<sup>a</sup>, Alice E. Milne<sup>a</sup>, Lindsay C.  
6 Todman<sup>a</sup>, A. Gordon Dailey<sup>a</sup>, Margaret J. Glendining<sup>b</sup>, Andrew P.  
7 Whitmore<sup>a</sup>

8 <sup>a</sup> Sustainable Agriculture Sciences department, <sup>b</sup> Computational and Analytical Sciences  
9 department, Rothamsted Research, Harpenden, Hertfordshire, AL5 2JQ, UK

10

11 *Keywords: Modelling, crops, soil processes, nutrient flow, water movement, agriculture*

12

13 \*Corresponding author

14 E-mail address [alice.milne@rothamsted.ac.uk](mailto:alice.milne@rothamsted.ac.uk)

15

16 HIGHLIGHTS

- 17 • Understanding trade-offs between yield and environment is essential for SI
- 18 • The Landscape Model aids the understanding of crop-soil-water interactions
- 19 • Model validated against 50 years of data from two long-term experiments
- 20 • Model validated against spatially-explicit data from the North Wyke farm platform
- 21 • The model simulated wheat yield, grain N and grain P particularly well

22

23

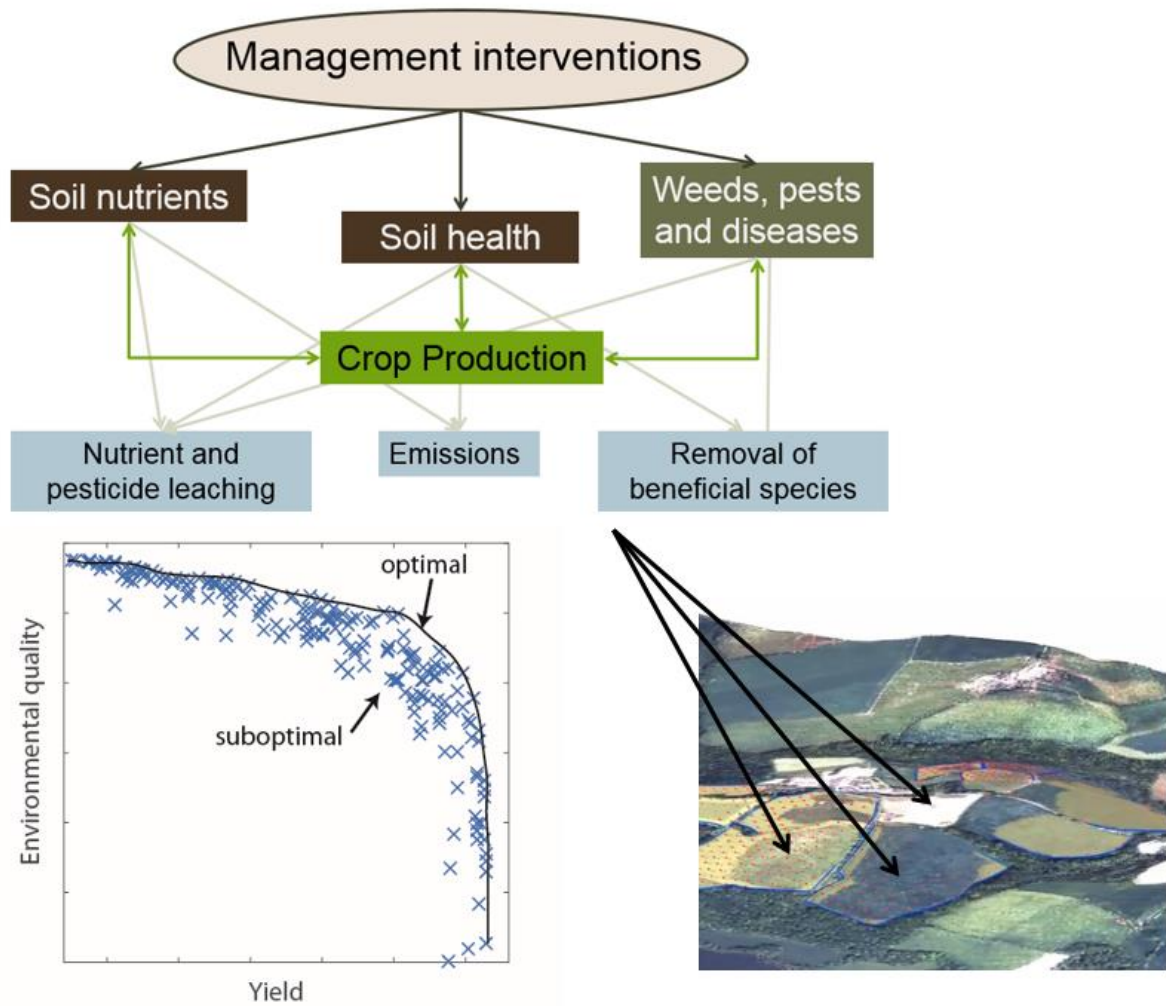
24 ABSTRACT

25 We describe a model framework that simulates spatial and temporal interactions in agricultural  
26 landscapes and that can be used to explore trade-offs between production and environment so  
27 helping to determine solutions to the problems of sustainable food production. Here we focus  
28 on models of agricultural production, water movement and nutrient flow in a landscape. We  
29 validate these models against data from two long-term experiments, (the first a continuous  
30 wheat experiment and the other a permanent grass-land experiment) and an experiment where  
31 water and nutrient flow are measured from isolated catchments. The model simulated wheat  
32 yield (RMSE 20.3-28.6%), grain N (RMSE 21.3-42.5%) and P (RMSE 20.2-29% excluding  
33 the nil N plots), and total soil organic carbon particularly well (RMSE 3.1 – 13.8%), the  
34 simulations of water flow were also reasonable (RMSE 180.36 and 226.02). We illustrate the  
35 use of our model framework to explore trade-offs between production and nutrient losses.

36

37

38



## 43 **1. Introduction**

44           Increasingly, agricultural production is being compelled to look not just at its  
45 externalities such as the environmental pollution or depletion of natural resources but also at  
46 the provision of wider ecosystem services such as biodiversity. Schemes to monitor or assess  
47 land for all of these factors are prohibitively expensive and yet there is a need to analyse modern  
48 agricultural systems for the purposes of policy, planning or management. Not surprisingly  
49 therefore, computer simulation models have a role to play in filling the large gaps between  
50 what we need to know and what is available from measurements.

51           Simulation models of agricultural systems abound, some focussing on specific aspects  
52 such as soil organic matter dynamics (Coleman et al., 1997), crop growth (Semenov and  
53 Stratonovitch, 2015), water movement (Addiscott and Whitmore, 1991), emissions (Rolston et  
54 al., 1984), competing organisms (Andrew and Storkey, 2017), and some integrating to  
55 agricultural management systems (Brisson et al., 2003; Keating et al., 2003). Others focus on  
56 the natural systems, tracing biodiversity often quite specifically (Andam et al., 2008; Koh et  
57 al., 2010). Some models, particularly agricultural ones, focus on field (Bell et al., 2012; Parton  
58 et al., 1994) or farm scales (Del Prado et al., 2011). Biodiversity models often focus on larger  
59 scales and water management models are naturally focussed on river basins or catchments  
60 (Whitehead et al., 2014).

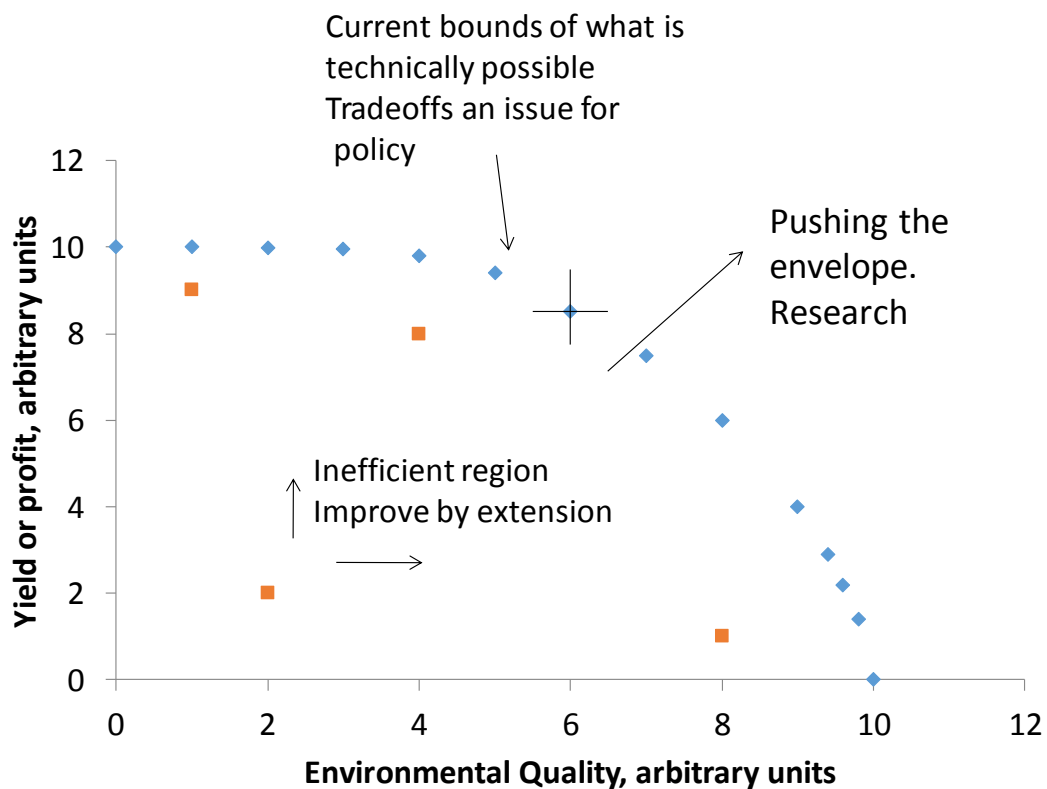
61           Many models simulate fields or regions, some simulate particular fluxes, say water  
62 from land to rivers. It is rarer to find models that try to integrate several of the impacts of  
63 farming in the landscape, and those that do adopt a relatively empirical, data-driven approach  
64 (Jackson et al., 2013; Tilman et al., 2001) that makes it difficult to explore the interactions  
65 between components of that landscape that might be better managed with a more holistic  
66 overview. It is rarer still to find models that make explicit spatial and temporal linkage between

67 adjacent fields and integrate all aspects of the managed farm environment up to the catchment  
68 level. Such a model would be useful to understand the spatial interactions and impact of the  
69 natural (weeds, pest and diseases) as well as management (irrigation, fertilizer and application  
70 of pesticides) events on an agricultural landscape. Our aim is to develop a spatially explicit  
71 model that can simulate the essential processes of soil, water, crop growth and biodiversity for  
72 agricultural landscapes in the UK. This model can then be used to understand the trade-off  
73 between farm management practices on farm economy and the environment. The ability to  
74 quantify such trade-offs is critical to our management of the landscape and underpins many  
75 sustainability frameworks including the three pillars of sustainability (environmental,  
76 economic and social), the UN Sustainable Development goals which includes several targets  
77 that relate to agricultural landscapes (Gil et al., 2017), and water-energy-food nexus approaches  
78 that aim to consider the use of all of these resources. While tradeoff models exist (e.g. see  
79 Sharps et al., 2017) they usually operate at large scales, not accounting for the field or farm  
80 scale at which land management decisions are often made. These models are often focussed on  
81 land-use options within in GIS-based systems, operate on annual time-scales and can be  
82 focussed on policy. Our approach, and ultimate aim, is to simulate interactions between the  
83 multiple processes that take place in agricultural fields and the farmed landscape with a view  
84 to uncovering strategies for development and improvement of agri-environmental systems,  
85 beyond the current envelope (Fig 1). By working on a daily time-step we can simulate the  
86 processes and inform the decisions that someone who manages land will have to take.

87         Here we report the first version of our model that integrates agricultural production,  
88 water movement and nutrient flow in a landscape. The model combines aspects of several  
89 published model [RothC (Coleman and Jenkinson, 2014), LINTUL (Wolf, 2012), SUCROS  
90 (van Laar et al., 1997), and Century (Parton et al., 1994)], but also includes novel factors that  
91 have been implemented to capture potential improvements in yield that result from

92 management actions. These include coupling the RothC model to include the dynamics of N  
 93 and P and responses to changes in bulk-density that result from changes in soil organic matter.  
 94 We evaluate the model against data on crop growth and nutrient uptake for cereals and for  
 95 grass, and the integration in space of water and nutrients leaving agricultural fields. We then  
 96 illustrate how our model can be used to explore trade-offs between production and environment  
 97 with a scenario based on a wheat crop grown in conditions typical of arable England.

98



99

100 Fig1: Representation of an environmental-economic production possibility frontier.

101 The blue diamonds are independent outcomes of management that optimises both yield and  
 102 environmental quality at the same time. A decision along this line is a matter for policy. The  
 103 orange squares within the envelope are inefficient in the sense that either production or  
 104 environmental quality could be improved without impacting the other. This is the region for  
 105 extension. Beyond the envelope is a zone where outcomes are currently infeasible and this is



106 the area which research addresses. An origin placed over any point (for example the cross  
107 shown in the figure on the middle of the envelope), facilitates the definition of the envelope  
108 algorithmically: if another point can be found in the first quadrant (North East) then the first  
109 point is not on the envelope.

110

## 111 **2. Methodology**

112 Our intention was to build a model system capable of exploring the multiple interactions  
113 between components of a simple landscape and to take into account both within and between  
114 field movement of components such as water and nitrate. Nonetheless, because we wished to  
115 build a system that can be used on a reasonably large landscape comprising many fields and  
116 boundaries, we based our system on simple but adequate descriptions of the processes involved.  
117 Here we report on interactions and differences between single or adjacent but joined fields and  
118 focus our discussion on productivity and loss of water and nitrogen to water courses and the  
119 atmosphere. To do so we describe an integrated model of crop, water and soil processes that  
120 runs on a daily time step. We validate this using data from the Broadbalk and Park Grass long-  
121 term experiments at Rothamsted Research, in Harpenden, SE England, and spatial interactions  
122 are tested on data from the more recently established North Wyke Farm Platform, at  
123 Rothamsted Research, near Okehampton, SW England (Orr et al., 2016).

124

### 125 *2.1 Spatial structure*

126 We impose a grid on the landscape where, dependant on size, each field is represented  
127 by one or more grid cells. Soil properties are set in each cell and initial values are given for  
128 bulk density, pH and soil water. Within each cell we model crop growth, the dynamics of soil  
129 water, total soil organic carbon (TOC), changes in bulk density and nutrient flows on a daily

130 time step. In cases where fields are made up of several cells, water and nutrients can move  
131 laterally between cells, as well as vertically through the soil profile. This model structure allows  
132 us to explore both temporal and spatial interactions. Cell edges can be designated as ditches  
133 (into which water and nutrients may flow), hedgerows or field margins.

134

## 135 *2.2 Soil water*

136 The soil water model uses a capacity based approach (Addiscott and Whitmore, 1991;  
137 Van Ittersum et al., 2003; van Laar et al., 1997). The soil is divided into three layers. This  
138 choice is a compromise between capturing the heterogeneity of the soil profile (which would  
139 require multiple layers in the simulation) and minimising complexity to enable fast run-times  
140 which are important when coupling models with optimisation algorithms over large spatial  
141 scales. In our study each layer was initially set to 230mm. The capacity of each of the soil  
142 layers is calculated with van Genuchten (1980) soil water release curves determined using the  
143 HYPRES pedo-transfer functions (Wösten et al., 1999). These functions use texture, soil  
144 organic matter and bulk density to derive the water release curves. For the topsoil, these release  
145 curves are updated daily to take into account changes in bulk density, for example, when  
146 farmyard manure (FYM) is added (see section 2.6).

147 Infiltrating water fills the soil layers to field capacity (-10 kPa), and starting from the  
148 top layer, excess water drains to the layer below, with water draining from layer 3 becoming  
149 drainage. In addition to percolation, water is lost by runoff and evaporation from the soil  
150 surface, and transpiration by the growing crop. The water available for crop uptake at any time  
151 is equal to the quantity of water stored above wilting point (-1500 kPa) in the rooted soil profile.  
152 A detailed description of the soil water model can be found in van Laar et al. (1997), with our  
153 modifications described in section 2.7. The change in water content in each layer is derived

154 from the balance between inputs from precipitation, and outputs from drainage, runoff,  
155 evaporation and transpiration.

156 Working at the water catchment scale Bell et al. (2007) developed a simple algorithm  
157 for estimating the total surface water leaving a sloping (i.e. not uniform in the vertical  
158 dimension) region. The storage capacity ( $S$ ) of high zones is reduced in relation to the  
159 topographic gradient according to

$$160 \quad S = \left(1 - \frac{\bar{g}}{g_{\max}}\right) S_{\max} \quad 1$$

161 where  $S_{\max}$  is the maximum storage capacity,  $\bar{g}$  is the average gradient in the cell and  $g_{\max}$  is  
162 the upper limit on the gradient. By adopting this strategy on a grid cell basis, we increase the  
163 flow of water out of each cell compared to that if it were flat. Runoff moves from the highest  
164 cell to the lowest by moving between cells with neighbouring boundaries. The proportion of  
165 runoff allocated in each direction is determined by the relative magnitude of the downward  
166 slopes. Dissolved substances such as nitrate, move in proportion to the water.

167

### 168 *2.3 Soil total organic carbon, nitrogen and phosphorus*

169 The soil total organic carbon (TOC) model is based on the Rothamsted carbon model,  
170 RothC, (Coleman and Jenkinson, 2014). Soil total organic carbon is split into four active  
171 compartments and a small amount of inert organic matter (IOM). The four active compartments  
172 are Decomposable Plant Material (DPM), Resistant Plant Material (RPM), Microbial Biomass  
173 (BIO) and Humified Organic Matter (HUM). Each compartment decomposes by a first-order  
174 process with its own rate constant. The IOM compartment is resistant to decomposition.  
175 Decomposition of each of the four active pools is modified by rate modifying factors for

176 temperature, moisture and plant retainment. Full details of the model can be found in (Coleman  
177 and Jenkinson, 2014).

178 The dynamics of the soil organic nitrogen (SON) and phosphorus (SOP) are modelled  
179 in a similar way to the TOC dynamics, both SON and SOP have the same pool structure as the  
180 active TOC pools. To determine initial values for each TOC pool, the model is run to  
181 equilibrium so that the modelled TOC matches the initial measured TOC. The initial values of  
182 each of the SON and SOP pools are then determined using the TOC values, and the C:N and  
183 C:P ratios of each pool. The  $C:N_{\text{Bio}}$  and  $C:N_{\text{Hum}}$  ratios are both fixed at 8.5 (Bradbury et al.,  
184 1993), whereas  $C:N_{\text{DPM}}$  and  $C:N_{\text{RPM}}$  ratios vary over time depending on the carbon inputs to  
185 soil from the crop or the addition of organic amendments. The  $C:P_{\text{Bio}}$  and  $C:P_{\text{Hum}}$  ratios are  
186 fixed at 50.0 and 100.0 respectively, like nitrogen the  $C:P_{\text{DPM}}$  and  $C:P_{\text{RPM}}$  ratios vary over  
187 time depending on the carbon inputs to the soil from the crop or the addition of organic  
188 amendments.

189 The N in pool  $i$  that is mineralised or immobilized is given by

$$190 \quad M_i = \frac{\Delta_i}{\rho_i} - \frac{B_i}{\rho_{\text{Bio}}} - \frac{U_i}{\rho_{\text{Hum}}} \quad 2$$

191 where  $\Delta_i$  is the change in pool  $i$  from day  $t$  to  $t + 1$ ,  $B_i$  is the amount of pool  $i$  transformed  
192 to biomass from day  $t$  to  $t + 1$ ,  $U_i$  is the amount of pool  $i$  transformed to humus from day  $t$  to  
193  $t + 1$ ,  $\rho_i$  is the C:N ratio for pool  $i$ , and  $\rho_{\text{Bio}}$  and  $\rho_{\text{Hum}}$  are the C:N ratios for the biomass and  
194 humus pools respectively. The sum of  $M_i$  across the four pools gives the net mineralisation or  
195 immobilisation, if the sum of  $M_i$  is negative immobilisation occurs and mineral N is removed  
196 from the soil, if the sum of  $M_i$  is positive mineralisation occurs and mineral N is added as  
197  $\text{NH}_4^+$  to the soil. If there is not enough soil mineral N ( $\text{NO}_3^-$  and  $\text{NH}_4^+$ ) on a particular day, then

198 decomposition of TOC does not happen. If there is enough soil mineral N, then N is removed  
199 from the  $\text{NH}_4^+$  pool in preference to  $\text{NO}_3^-$  pool.

200 The P mineralisation or immobilization of each SOP pool is calculated in a similar way  
201 to the mineralisation N, where in Equation (2),  $\rho_i$  is the C:P ratio for pool  $i$ , and  $\rho_{\text{Bio}}$  and  $\rho_{\text{Hum}}$   
202 are the C:P ratios for the biomass and humus pools respectively. When P is mineralised 80%  
203 is added to the available P pool, and the remaining 20% is added to the non-available P pool.  
204 For P 80% of mineralised P is added to or subtracted from the available P pool, similarly when  
205 immobilization of P occurs 80% is taken from the available P pool, and the remaining 20% is  
206 taken from the non-available P pool (see section 2.5).

207

#### 208 2.4 Soil Mineral Nitrogen

209 In the model, soil mineral N consists of N in ammonium ( $\text{NH}_4^+$ ) and nitrate ( $\text{NO}_3^-$ ).  
210 Inputs of N through atmospheric deposition ( $N_{\text{AtDep}}$ ) were set to 35 kg N yr<sup>-1</sup> (Anon, 1998) for  
211 the UK in 1966, decreasing linearly to 20 kg N yr<sup>-1</sup> in 2012 (pers. comm. Goulding). Like,  
212 Sundial (Anon, 1998) it was distributed evenly throughout the year as nitrate. Nitrogen applied  
213 as fertilizer enters the  $\text{NH}_4^+$  or  $\text{NO}_3^-$  pools depending on the type of fertilizer applied. When  
214 organic amendments are added, N enters the soil inorganic nitrogen pools by mineralisation  
215 (see section 2.3).

216 Rainfall runoff mixes in the model with the water and minerals in the top 20 mm of the  
217 soil profile. The amount of mineral nitrogen ( $\text{NH}_4^+$  and  $\text{NO}_3^-$ ) in runoff from the the top 20 mm  
218 of soil ( $N_{\text{Run}}$ ) is given by (Sharpley, 1985)

$$219 \quad N_{\text{Run}} = \frac{N_{\text{Surf}} W_{\text{Run}}}{W_{\text{Run}} + W_{\text{Surf}}} \quad 3$$

220 where the surface water ( $W_{\text{Surf}}$ ) is given by difference in the volumetric water content at  
 221 saturation and air dried, multiplied by 20 to give the water (mm) in the top 20 mm,  $W_{\text{Run}}$  is  
 222 the water runoff (mm) and the surface N ( $N_{\text{Surf}}$ ) is given by

$$223 \quad N_{\text{Surf}} = \frac{20}{\delta(1)} (N_{\text{NH}_4} + N_{\text{NO}_3}) \quad 4$$

224 where  $\delta(1)$  is the depth of the first layer.

225 Any nitrate in the soil can potentially move down the soil profile with the water. The  
 226 concentration of  $\text{NO}_3^-$  in layer  $l$ , ( $\gamma_{\text{NO}_3}(l)$ ) is given by:

$$227 \quad \gamma_{\text{NO}_3}(l) = \frac{N_{\text{NO}_3}(l)}{W(l)} \quad 5$$

228 where  $N_{\text{NO}_3}(l)$  is the  $\text{NO}_3^-$  ( $\text{kg N ha}^{-1}$ ) in layer  $l$ ,  $l = 1 \dots 3$ , and  $W(l)$  is the water content of  
 229 layer  $l$ .

230 The amount of  $\text{NO}_3^-$  ( $\text{kg N d}^{-1}$ ) that moves down each layer  $l$  is given by

$$231 \quad F_{\text{NO}_3}(l) = \max(0, \min\{N_{\text{NO}_3}(l), \gamma_{\text{NO}_3}(l)F_W(l+1)\}) \quad 6$$

232 where  $F_W(l)$  is the water that flows from layer  $l$  to layer  $l+1$ . The nitrate that moves down  
 233 from layer 3,  $F_{\text{NO}_3}(3)$ , is N leached out of the profile.

234 Nitrification is an aerobic process whereby the  $\text{NH}_4^+$  in the soil is oxidised to form  $\text{NO}_3^-$   
 235 and  $\text{N}_2\text{O}$ . Our models are based on Milne et al. (2005) and Parton et al. (2001). The rate of  
 236 nitrification depends on the soil properties, such as water filled pore space  $\theta/\theta_{\text{Sat}}$ , soil  
 237 temperature (T), soil moisture (M), and pH ( $S_{\text{pH}}$ ). In the model the amount of  $\text{N}_2\text{O}$  ( $\text{kg N ha}^{-1}$   
 238  $\text{day}^{-1}$ ) produced from a given amount of  $\text{NH}_4^+$  ( $N_{\text{NH}_4}(l)$ ) in layer  $l$  is given by

$$239 \quad N_{\text{N}_2\text{O}}(l) = k_{\text{N}_2\text{O}} N_{\text{NH}_4}(l) S_{\text{pH}}(l) \left(1 - \frac{\theta}{\theta_{\text{Sat}}(l)}\right), \quad 7$$

240 where  $k_{\text{N}_2\text{O}}$  is a constant that takes the value 0.0001. The amount of nitrate ( $\text{kg N ha}^{-1} \text{day}^{-1}$ )  
 241 produced from soil  $\text{NH}_4^+$  is given by

242 
$$N_{\text{NO}_3}(l) = \max[(N_{\text{NH}_4}(l) - N_{\text{N}_2\text{O}}(l) - N_{\text{min}})(1 - e^{-k}) f(T(l))g(M(l)), 0]$$
 8

243 where  $N_{\text{min}}$  is the minimum amount of  $\text{NH}_4^+$  that must be in the soil for nitrification to occur  
 244 (we assume  $N_{\text{min}} = 0.05$ ),  $k$  is a constant for nitrification which is set at 0.15, and  $f(T)$  and  
 245  $g(M(i))$  are functions that describe the effect respectively of temperature and moisture on  
 246 nitrification, for details see Godwin and Allan Jones (1991).

247 Denitrification is an anaerobic process whereby the  $\text{NO}_3^-$  in the soil is reduced to nitrous  
 248 oxide and nitrogen. The amounts of these gases produced depends on the soil conditions, most  
 249 notably the nitrate in the soil ( $N_{\text{NO}_3}$ ,  $\text{kg ha}^{-1}$ ), the water filled pore space ( $\theta/\theta_{\text{Sat}}$ ), soil  
 250 temperature ( $T$ ,  $^{\circ}\text{C}$ ), soil organic carbon ( $c$ ) and pH ( $S_{\text{pH}}$ ) (Del Grosso et al., 2000; Milne et al.,  
 251 2011; Nömmik, 1956). The effect of soil organic carbon on emissions is felt indirectly as a  
 252 result of the temperature function  $g(T)$ . We assumed the following simple model to describe  
 253  $\text{N}_2\text{O}$  emissions ( $\text{kg N ha}^{-1} \text{ day}^{-1}$ )

254 
$$\text{N}_2\text{O} = aN_{\text{NO}_3}f(\theta/\theta_{\text{Sat}})g(T)$$
 9

255 where  $a$  is a constant. We took the functional forms of  $f(\theta/\theta_{\text{Sat}})$  and  $g(T)$  from the literature  
 256 and then fitted the model parameters to data from field experiments from around the UK where  
 257 nitrate, soil temperature, water filled pore space, and  $\text{N}_2\text{O}$  emissions ( $\text{kg N ha}^{-1} \text{ day}^{-1}$ ) were  
 258 measured. Similar to other empirical or semi-empirical models, these parameter values can  
 259 only be assumed to hold for the range of conditions for which they were fitted, and outside of  
 260 this range further validation would be required. Nitrous oxide is linearly related to nitrate  
 261 ( $N_{\text{NO}_3}$ ) and we used the function defined by Lark and Milne (2016) to describe the effect of  
 262 water-filled-pore space on  $\text{N}_2\text{O}$  emissions. That is

263 
$$f(w) = \exp \left[ -0.6151 \left( \log \left\{ \frac{\theta/\theta_{\text{Sat}}(l)}{1 - \theta/\theta_{\text{Sat}}(l)} \right\} - 1.19 \right)^2 \right]$$
 10

264 where  $\theta/\theta_{\text{Sat}}(l)$  is the water filled pore space in each layer  $l$ . Data from Nömmik (1956)  
 265 suggested that the relationship between temperature and  $\text{N}_2\text{O}$  emissions should follow a normal  
 266 distribution with mean 23.65 and standard deviation 5.53. However, data from the Defra project  
 267 AC0116 (<http://www.environmentdata.org/archive/ghgno:676>) which we used to relate  
 268 average temperature to emissions, did not conform to the standard deviation given by Nömmik  
 269 (1956). Therefore, we assumed the same mean but fitted the standard deviation to our field  
 270 data. Our fitted model was

$$271 \quad \text{N}_2\text{O} = 0.000735 N_{\text{NO}_3} \exp[-0.6151(\theta/\theta_{\text{Sat}}(l) - 1.19)^2] \exp[-0.00045(T - 23.65)^2] \quad 11$$

272 which we apply in only the top two layers of our model as there is not sufficient biological  
 273 activity for denitrification to occur in the bottom soil layer.

274 When water filled pore space increases, the soil becomes more anaerobic and so the  
 275 amount of  $\text{N}_2$  produced increases. A similar relationship holds for temperature (Nömmik,  
 276 1956). We used the following model and fitted the parameters so that our model gave  
 277 proportions of  $\text{N}_2\text{O}$  to  $\text{N}_2$  similar to those observed in Colbourn (1988)

$$278 \quad \text{N}_2 = \frac{0.0052 N_{\text{NO}_3}}{(1 + e^{-0.14975(T+4.0)})(1 + e^{-12.0(\theta/\theta_{\text{Sat}}(l)-0.62)})} \quad 12$$

279 The nitrogen taken up by the crop each day is taken from the nitrate pool with an upper limit  
 280 of 6 kg N ha<sup>-1</sup> day<sup>-1</sup> (Semenov et al., 2007).

281

## 282 *2.5 Mineral Phosphorus*

283 In the model, mineral phosphorus is split into two pools: available P (which includes  
 284 phosphorus in soil solution and loosely adsorbed to the clay surface) and non-available P.



285 Eighty percent of the fertilizer P enters the available P pool and the remaining 20% enters the  
 286 non-available P pool (Wolf et al., 1987).

287 Similar to the N model, a proportion of the available P contained in the top 20 mm of  
 288 soil can be lost through runoff.

$$289 \quad P_{\text{Run}} = \frac{P_{\text{Surf}} W_{\text{Run}}}{W_{\text{Run}} + W_{\text{Surf}}} \quad 13$$

290 where the surface P ( $P_{\text{Surf}}$ ) is given by

$$291 \quad P_{\text{Surf}} = \frac{20}{\delta(1)} P_{\text{M}} \quad 14$$

292 where  $P_{\text{M}}$  is the mobile (dissolved and particulate) P which we assume to be 10% of  $P_{\text{AV}}$ . We  
 293 set solution P to 1% of the available P (pers. comm. Paul Poulton). This can potentially be  
 294 leached when water flows down the profile.

295 The soil organic P that is mineralised is added to the available P pool. Mineral P may  
 296 also be immobilised, in which case it is taken from the available P pool first and then from the  
 297 non-available P pool.

298 Available P ( $P_{\text{AV}}$ ) is converted to non-available P ( $P_{\text{NonAv}}$ ) by reversible processes  
 299 which reduce its extractability. In the model, the P content for each soil layer (available and  
 300 non-available P), which we define  $P_{\text{Tot}}$ , is calculated in  $\text{mg kg}^{-1}$  soil. The release to fixation  
 301 variable,  $V(l)$ , for layer  $l$  is given by

$$302 \quad V(l) = \begin{cases} \frac{\alpha_b P_{\text{Tot}}(l) + \beta_b}{P_{\text{Tot}}(l)}, & P_{\text{Tot}}(l) > \frac{\beta_a - \beta_b}{\alpha_b - \alpha_a} \\ \frac{\alpha_a P_{\text{Tot}}(l) + \beta_a}{P_{\text{Tot}}(l)}, & P_{\text{Tot}}(l) \leq \frac{\beta_a - \beta_b}{\alpha_b - \alpha_a} \end{cases} \quad 15$$

303  
 304 where  $\alpha_b$  and  $\beta_b$  are the slope and intercept, of value 0.113 and  $-49.3$  respectively, for the  
 305 linear relationship between  $P_{\text{AV}}$  and  $P_{\text{Tot}}$ . For small values of  $P_{\text{Tot}}$ , an alternative set of

306 coefficients  $\alpha_a$  and  $\beta_a$ , of value 0.0201 and  $-5.1$ , are used (see supplementary Fig. 1). The  
 307 ratio of release to fixation is given by

$$308 \quad R_{\text{RF}}(l) = \frac{V(l)}{1.0 - V(l)} \quad 16$$

309 The transfer of P from the non-available to the available pool  $P_{\text{NA} \rightarrow \text{Av}}$ , and the reverse transfer  
 310  $P_{\text{Av} \rightarrow \text{NA}}$  in layer  $l$  on day  $t + 1$  are given by

$$311 \quad P_{\text{NA} \rightarrow \text{Av}} = R_{\text{RF}}(l) P_{\text{Av}}(l; t) f_{\text{pH}}(S_{\text{pH}}(l)) \quad 17$$

$$312 \quad P_{\text{Av} \rightarrow \text{NA}} = \lambda P_{\text{NonAv}}(l; T) R_{\text{RF}}(l) f_{\text{pH}}(S_{\text{pH}}(l)), \quad 18$$

313 and so

$$314 \quad P_{\text{NonAv}}(l; t + 1) = P_{\text{NonAv}}(l; t) + P_{\text{Av} \rightarrow \text{NA}} - P_{\text{NA} \rightarrow \text{Av}} \quad 19$$

$$315 \quad P_{\text{Av}}(l; t + 1) = P_{\text{Av}}(l; t) - P_{\text{Av} \rightarrow \text{NA}} + P_{\text{NA} \rightarrow \text{Av}} \quad 20$$

316 The constant  $\lambda$  determines the rate of re-equilibration between  $P_{\text{Av}}$  and  $P_{\text{NonAv}}$  following the  
 317 addition of mineral P, and is set to 0.01 giving a half-life of approximately 65 days. The values  
 318 of coefficients,  $\alpha$ ,  $\beta$  and  $\lambda$  were established for a silty clay loam soil at Rothamsted. The rate  
 319 modifying function  $f_{\text{pH}}$  linearly increases from 0.0 to 1.0 as pH increases from 0 to 7, and then  
 320 linearly decreases back to zero as pH increases from 7 to 14. The P required by the crop is  
 321 taken from the available P pool, up to a limit of  $2 \text{ kg P ha}^{-1} \text{ day}^{-1}$ .

322

### 323 *2.6 Bulk density*

324 To take into account changes in depth caused by changes in bulk density as a result of,  
 325 for example, the addition of FYM, we used the Rawls (1983) nomogram to estimate bulk  
 326 density in relation to sand, clay and organic carbon contents of soil. The depth of the topsoil is

327 modified to reflect the change in bulk density (changes in depth and bulk density only occur in  
328 the top soil). Because of the changes in depth and bulk density in the top soil, we modify water  
329 properties, such as the water content at saturation, field capacity, and wilting point, daily (see  
330 section 2.2). Modelling bulk density dynamically in this way has been described previously by  
331 Whitmore et al. (2011).

332

### 333 2.7 Crop model

334 Our crop model is a generic plant growth model, which uses a light use efficiency (LUE,  
335 g dry matter MJ<sup>-1</sup>) based approach to calculate the biomass production (Monteith, 1990;  
336 Monteith and Moss, 1977). The rate of biomass ( $B_{\text{crop}}$ ) produced each day is given by

$$337 \quad \frac{dB_{\text{crop}}}{dt} = Q \varepsilon W_{\text{rf}} N_{\text{NI}} P_{\text{NI}} \quad 21$$

338 where  $Q$  is the intercepted PAR (MJ PAR m<sup>-2</sup> surface area) which depends on the solar  
339 radiation and canopy leaf area,  $\varepsilon$  is the crop specific LUE, which for grass, changes with  
340 development stage see Schapendonk et al. (1998),  $W_{\text{rf}}$  is the transpiration reduction factor,  
341  $N_{\text{NI}}$  and  $P_{\text{NI}}$  are the nitrogen and phosphorus nutrition indices, which range from zero to one.  
342 For grass, LUE is reduced for higher radiation levels (Schapendonk et al., 1998). In our model  
343 LUE is reduced by a factor  $R_{\text{LUE}}$  which decreases from 1.0 to 0.33 when radiation increases  
344 from 10 to 40 MJ m<sup>-2</sup> d<sup>-1</sup>. Schapendonk et al. (1998) also modified LUE, by the temperature  
345 factor  $T_{\text{LUE}}$ , which in this study increases linearly from 0.0 to 1 between 6.0 and 9.0 °C. The  
346 biomass formed is partitioned between roots, stem, leaves and storage organs based on the  
347 development stage (DVS) (Boons-Prins et al., 1993; Wolf, 2012).

348 The transpiration reduction factor ( $W_{\text{rf}}$ ) is defined as the ratio of actual transpiration  
349 (mm day<sup>-1</sup>) to potential transpiration (mm day<sup>-1</sup>) and is calculated

350 
$$W_{rf} = \frac{\sum_{l=1}^3 A_{Tran}(l)}{P_{Tran}} \quad 22$$

351 where  $P_{Tran}$  is the daily potential transpiration which is calculated as in Lintel (Wolf, 2012).

352 The amount of the actual transpiration coming out of layer (l) is given by

353 
$$A_{Tran}(l) = \frac{P_{Tran}(l) W_S(l)^2 F_{RL}(l)}{W_S(1) F_{RL}(1) + W_S(2) F_{RL}(2) + W_S(3) F_{RL}(3)}. \quad 23$$

354 Here  $F_{RL}$  is the fraction of root in each layer and  $W_S$  is the impact of water content on the  
 355 water stress function. This follows the approach of Li et al. (2001). This impact of water content  
 356 is based on the method described in Feddes et al. (1976) given by

357 
$$W_S = \begin{cases} \frac{\theta_s - \theta}{\theta_s - \theta_a}, & \text{for } \theta > \theta_a \\ 1 & \text{for } \theta_a \geq \theta > \theta_d \\ \frac{\theta - \theta_w}{\theta_d - \theta_w}, & \text{for } \theta_d \geq \theta > \theta_w \end{cases} \quad 24$$

359 where  $\theta$  is the volumetric water content,  $\theta_s$  is the water content at saturation,  $\theta_a$  is the water content  
 360 at  $-5$  kPa,  $\theta_d$  is the water content at  $-40$  kPa, and  $\theta_w$  is the water content at wilting point ( $-1500$   
 361 kPa). Water stress affects grass less than arable crops (per comms J. Storkey). In simulations,  
 362 when the soil is saturated grass does not suffer water stress. When the volumetric water content  
 363 falls below  $\theta_d = -40$  kPa the water stress factor  $W_S$  decreases linearly between  $\theta_d$  and  $\theta_w$  to 0.4.

364

365 The proportion of root ( $F_{RL}$ ) in each layer  $l$  is given by

366 
$$F_{RL}(l) = \frac{R_{Len}(l)}{R_{Len}(1) + R_{Len}(2) + R_{Len}(3)} \quad 25$$

367 where  $R_{Len}$  is the root length per unit area ( $\text{mm mm}^{-2}$ ).

368 The root depth ( $d_{root}$ ) increases by 12.0 mm per day to a maximum root depth which  
 369 depends on the crop being modelled. The root length per unit area within each layer, calculated  
 370 according to an adaptation of the method of Gerwitz and Page (1974), is given by

371 
$$R_{\text{Len}}(l) = -\frac{R_0}{a (e^{-a z_2(l)} - e^{-a z_1(l)})} \quad 26$$

372 where  $R_0$  is the root length density at the soil surface ( $\text{mm mm}^{-3}$ ) the value of which is non-  
 373 essential to the model as it cancels out in Equation (25),  $z_1(l)$  and  $z_2(l)$  are the upper and  
 374 lower horizon depth (mm) of layer  $l$ , and  $a$  is given by

375 
$$a = -\frac{\ln(1 - F_r)}{d_{\text{root}}} \quad 27$$

376 where  $F_r$  is the fraction (arbitrarily defined as 0.98) of the root length that is present above  
 377  $d_{\text{root}}$ .

378 The uptake of plant nutrient (N and P) is determined by the crop demand and the supply  
 379 of these nutrients by soil. The total nutrient demand of the crop is the sum of the nutrient  
 380 demand from its individual organs (i.e. roots, stems and leaves excluding storage organs, for  
 381 which nutrient demand is met by translocation from the other organs). Nutrient demand of the  
 382 individual organs is calculated as the difference between maximum and actual organ nutrient  
 383 contents. The maximum nutrient content is defined as a function of canopy development stage.  
 384 The total nutrient uptake of the crop takes place before anthesis. Sub-optimal nutrient  
 385 availability in the soil leads to nutrient stress in the crop. A detailed description of crop nitrogen  
 386 dynamics is reported by Shibu et al. (2010) and P dynamics follows N in a similar way.

387 Nitrogen stress in the plant growth model is expressed as nitrogen nutrition index ( $N_{\text{NI}}$ )  
 388 and is calculated by:

389  
 390 
$$N_{\text{NI}} = \max \left[ 0, \min \left( 1, \frac{N_{\text{leaf}} + N_{\text{stem}} - N_{\text{Res}}(\Omega_{\text{leaf}} + \Omega_{\text{stem}})}{\Omega_{\text{leaf}} N_{\text{MaxPropleaf}} + \Omega_{\text{stem}} N_{\text{MaxPropstem}} - N_{\text{Res}}(\Omega_{\text{leaf}} + \Omega_{\text{stem}})} \right) \right] \quad 28$$

391 where  $N_{\text{leaf}}$  and  $N_{\text{stem}}$  are the  $N$  in the leaf and stem respectively,  $\Omega_{\text{leaf}}$  and  $\Omega_{\text{stem}}$  are the  
 392 weights of the leaf and stem respectively,  $N_{\text{MaxPropleaf}}$  and  $N_{\text{MaxPropstem}}$  are the maximum  
 393 proportion of  $N$  in the leaf and stem respectively. The residual  $N$  ( $N_{\text{Res}}$ ) is the fraction of  $N$

394 which is part of the cell structure and was fixed at 0.004 for wheat (Wolf, 2012) and 0.01 for  
 395 grass (Bouman et al., 1996). For wheat, the maximum N in the leaf is given by:

$$396 \quad N_{\text{MaxPropleaf}} = 0.046 \exp(-1.7D) + 0.014 \quad 29$$

397 where  $D$  is the development stage of the crop which is calculated using thermal time modified  
 398 by a vernalisation factor and the photosensitivity of the crop (see Wolf (2012), and references  
 399 therein). For grass we set  $N_{\text{MaxPropleaf}}$  to 0.0425. The maximum N in the stem is given by  
 400  $N_{\text{MaxPropStem}} = 0.5 N_{\text{MaxPropLeaf}}$ , (see Wolf (2012)).

401 The phosphorus nutrition index ( $P_{\text{NI}}$ ) is calculated by:

$$402 \quad P_{\text{NI}} = \max \left[ 0, \min \left( 1, \frac{P_{\text{leaf}} + P_{\text{stem}} - (\Omega_{\text{leaf}} P_{\text{ResLeaf}} + \Omega_{\text{stem}} P_{\text{ResStem}})}{\Omega_{\text{leaf}} P_{\text{MaxPropleaf}} + \Omega_{\text{stem}} P_{\text{MaxPropstem}} - N_{\text{Res}} (\Omega_{\text{leaf}} P_{\text{ResLeaf}} + \Omega_{\text{stem}} P_{\text{ResStem}})} \right) \right] 30$$

403 where  $P_{\text{leaf}}$  and  $P_{\text{Stem}}$  are the P in the leaf and stem respectively, and  $P_{\text{MaxPropleaf}}$  and  
 404  $P_{\text{MaxPropstem}}$  are the maximum proportion of P in the leaf and stem respectively. For wheat the  
 405 residual P in the leaf is  $P_{\text{ResLeaf}} = 0.0003$  and in the stem  $P_{\text{ResStem}} = 0.00018$ . For grass both  
 406  $P_{\text{ResLeaf}}$  and  $P_{\text{ResStem}}$  are set to 0.001 (Wolf et al., 1987). For wheat the maximum P in the  
 407 leaf reduces with development stage. From development stages 0 to 0.7 it reduces linearly from  
 408 0.0066 to 0.0036 and then from 0.0036 to 0.0009 from development stage 0.7 to 1, after which  
 409 it holds the value of 0.0009. For grass the maximum P in the leaf is fixed at 0.0035 (Bouman  
 410 et al., 1996).

411 Processes leading to the aboveground litter formation and carbon turnover below  
 412 ground are similar for both crops and grass but their rates are different. We assume that 50%  
 413 of the dead leaves become litter on a daily basis and the remainder is left on the stem. The rate  
 414 at which the roots die is a function of growth stage. In case of crops, the root death happens  
 415 towards the latter part of the growing season ( $\text{DVS} > 1.5$ ) at a rate of 0.02 per day. In case of

416 grass, once the root system has been established (3-6 months after sowing, DVS=0.01), root  
417 death becomes continuous at a rate of 0.01 per day. The root exudates are considered to be a  
418 part of root death, so are not modelled separately. The leaf death rate is a function of heat  
419 stress, nitrogen stress and shading as described in Schapendonk et al. (1998). All C, N, and P  
420 from dead roots and litter is returned to the soil.

421 The grass model differs somewhat from the crop model as grass has indeterminate  
422 growth and is not allowed to flower (so always has a DVS always < 1.0) as it can be cut or  
423 grazed in the model (unlike the crop which completes its life cycle in a given growing season).  
424 Grass is a perennial crop that grows for one or more seasons before being reseeded. Cut grass  
425 and grazed grass is removed from the modelled system. The amount removed is such that the  
426 remaining biomass cannot fall below 50 g m<sup>-2</sup>. Livestock deposit nutrients into the system as  
427 manure. When animals are on the field, we set the deposition of C and N for each animal type  
428 based on data from (Cottrill and Smith, 2007), for each beef animal this was 4.03 kg C of  
429 manure per day containing 0.22 kg N, for each dairy cow this was 6.45 kg C per day containing  
430 0.35 kg N, and for each sheep this was 0.45 kg C per day as fresh deposit, containing 0.02 kg  
431 N per day. These rates are multiplied by the stocking rate to give the rate of deposit per hectare.

432

### 433 *2.8 Data requirements*

434 For each layer of the soil, the model requires initial values for soil depth, clay, silt,  
435 TOC, bulk density, available P, non available P, soil NH<sub>4</sub>, soil NO<sub>3</sub>, soil pH. Initial values for  
436 elevation and latitude are also needed. The model runs with a daily time-step and so for each  
437 simulated day weather data (minimum and maximum temperature, rainfall, radiation, vapour  
438 pressure and windspeed) are needed. For each season and where relevant to the crop, sowing  
439 dates, fertilizer application timing, type and dose and dates when the grass is cut are required.

440

## 441 2.9 Case studies

442 To test our model, we used data from two long-term agricultural experiments and one  
443 more recent grass-livestock experiment. These were: The Broadbalk wheat experiment, and  
444 the Park Grass permanent grassland experiment at Rothamsted Research, Hertfordshire, UK  
445 ( $51.8^{\circ}$  N,  $0.37^{\circ}$  W), and the more recent North Wyke farm platform at Rothamsted Research,  
446 near Okehampton, UK ( $50.77^{\circ}$  N,  $3.92^{\circ}$  W), which has spatially integrated data from livestock-  
447 bearing grassland in a sloping terrain. We used a suite of statistical metrics (including the mean,  
448 standard deviation, root mean square error, and sample correlation coefficient,  $r$ ) to quantify  
449 the performance of our model (see Smith et al., 1997).

450

### 451 2.9.1 Broadbalk

452 The Broadbalk wheat experiment has been running since 1843, and wheat has been  
453 sown and harvested on all or part of the experiment every year since then. The original aim of  
454 the experiment was to test the effects of various combinations of inorganic fertilizers and  
455 organic manures on the yield of winter wheat. The experiment was divided into different strips  
456 given a range of fertilizer applications, which extended the whole length of the field. In 1926  
457 the experiment was divided into five Sections, crossing the fertilizer treatments at right angles,  
458 where each section was bare fallowed one year in five to control weeds. In 1968 the experiment  
459 was further divided into 10 Sections, so that the yield of wheat grown continuously could be  
460 compared with that grown in rotation after a two-year break. The plots receive management  
461 consistent with standard practice for the time. The soil is clay loam to silty clay loam,  
462 predominately Batcombe series (Avery and Catt, 1995), FAO classification: Chromic Luvisol  
463 (or Alisol), U.S. Soil Taxonomy: Aquic (or Typic) Paleudalf. The site is thought to have been



464 in arable cropping for many centuries before the start of the experiment. Further details are  
 465 available from <http://www.era.rothamsted.ac.uk/Broadbalk>

466 The plots from the continuous wheat sections (Section 1 and 9), selected for this study,  
 467 receive a range of fertilizer and FYM applications (see Table 1). Wheat has been grown every  
 468 year on these Sections, since 1966. Modern, short-strawed high yielding varieties were  
 469 introduced in the 1967–1968 season and it is from this date that we test the model. Most of the  
 470 data are available from the electronic Rothamsted Archive (eRA  
 471 <http://www.era.rothamsted.ac.uk>). Periodic measurements of TOC were made on all plots  
 472 (Watts et al., 2006; Pers. comm. P. Poulton for later data), measurements of volumetric water  
 473 content on plot 8 in 2007 (Pers. Comm, C. Watts) and measurements and estimates of N  
 474 leaching were made between 1990 and 1998 (Goulding et al., 2000). Grain N was measured  
 475 1968-2012, and grain P from 1968-2011 (except 1976-1985), Section 1 only.

476 Table 1. The fertilizer and manure treatments applied annually to the Broadbalk experiment  
 477 plots used in the simulations.

Plot	Treatments				
	up to 1967	1968 - 1984	1985 - 2000	2001 - 2004	2005 - 2012
3	Nil	Nil	Nil	Nil	Nil
5	P K Na Mg	P K Na Mg	P K Mg	K Mg	K Mg
6	48N P K Na Mg	48N P K Na Mg	48N P K Mg	48N K Mg	48N K Mg
7	96N P K Na Mg	96N P K Na Mg	96N P K Mg	96N K Mg	96N K Mg
8	144N P K Na Mg	144N P K Na Mg	144N P K Mg	144N K Mg	144N K Mg
9	48N* P K Na Mg	192N P K Na Mg	192N P K Mg	192N K Mg	192N K Mg
15	96N P K Na Mg	192N P K Na Mg	240N P K Mg	240N K Mg	240N K Mg
16	96N* P K Na Mg	96N P K Na Mg	288N P K Mg	288N K Mg	288N K Mg

2.1	FYM since 1885	FYM 96N	FYM 96N	FYM 96N	FYM 144N
2.2	FYM	FYM	FYM	FYM	FYM

---

478 The values of N are in kg N ha<sup>-1</sup>, applied as ammonium sulphate 1843-1967, as calcium  
479 ammonium nitrate between 1968-1985, and as ammonium nitrate thereafter. Treatments with  
480 \* were applied as sodium nitrate. Farmyard manure (FYM) was applied at 35 t ha<sup>-1</sup> fresh  
481 weight, and contains approximately 250kg N ha<sup>-1</sup>. Other elements were applied at 35 kg P  
482 ha<sup>-1</sup>, 90 kg K ha<sup>-1</sup>, 16 kg Na ha<sup>-1</sup> until 1973 and 12 kg Mg ha<sup>-1</sup> respectively. P has not been  
483 applied since 2001, due to high levels of plant available P in the soil. For more details see  
484 <http://www.era.rothamsted.ac.uk/Broadbalk>

485

486 We ran the model to simulate the plots listed in Table 1 using weather data from the  
487 Rothamsted meteorological station from 1966 to 2012. Comparisons were made between  
488 measured and simulated values of crop yield, content of N and P in the grain, TOC, volumetric  
489 water content and nitrate leaching.

490

### 491 2.9.2 *Park Grass*

492 The Park Grass experiment is the oldest experiment on permanent grassland in the  
493 world. Started by Lawes and Gilbert in 1856, its original purpose was to investigate ways of  
494 improving the yield of hay by the application of inorganic fertilizers and organic manure.  
495 Within 3 years it became clear that these treatments were having a dramatic effect on the  
496 species composition of what had been a uniform sward. The continuing effects of the original  
497 treatments on species diversity and on soil function, together with later tests of liming and  
498 interactions with atmospheric inputs and climate change (Storkey et al., 2015), has meant that  
499 Park Grass has become increasingly important to ecologists, environmentalists and soil

500 scientists. The soil is silty clay loam, predominately Hook series, with areas more typical of  
501 the Batcombe series (Avery and Catt, 1995), FAO Classification: Chromic Luvisol (or Alisol),  
502 U.S. Soil Taxonomy: Aquic (or Typic) Paleudalf. The site is known to have been in permanent  
503 pasture for at least 100 years before the start of the experiment. For further details see  
504 <http://www.era.rothamsted.ac.uk/Park>

505         The plots are cut in mid-June, and made into hay. A second cut is usually taken in the  
506 autumn, except in a few years, when there was insufficient herbage to sample. Since 1960,  
507 yields have been estimated from strips cut with a forage harvester. The remainder of the plot is  
508 still mown and made into hay, continuing earlier management. For the second cut, the whole  
509 of each plot is cut with a forage harvester. The experiment is never cultivated, and the site was  
510 in permanent grassland for at least 100 years before the experiment began. Further details are  
511 available from <http://www.era.rothamsted.ac.uk/Park>

512         Here we simulated two plots, Plot 3a and 14/2a, with contrasting fertilizer treatments.  
513 Plot 3a has received no inorganic fertilizer or manure since 1856. Plot 14/2a has received 96  
514 kg N ha<sup>-1</sup> in the spring, and 35 kg P in the autumn each year since 1858, plus K, Na and Mg.  
515 In 1965 the plots were divided into four subplots, given different amounts of chalk to maintain  
516 soil at pHs of 7, 6 and 5 (sub-plots a, b and c, respectively). The fourth sub plot (d) receives no  
517 chalk. We have selected sub-plot 'a' for this simulation, with a pH of 7. We use yield data from  
518 1966-2012, with two cuts each year except in 2003, when no second cut was taken, with  
519 weather data from the Rothamsted meteorological station.

520         We chose Plot 14/2a over the other N fertilizer plots because N is applied as sodium  
521 nitrate, whereas in most other plots N is applied as ammonium sulphate, which has an  
522 acidifying effect on the soil and so a dramatic effect on species composition and the  
523 decomposition of soil organic matter (see <http://www.era.rothamsted.ac.uk/Park>).

524

### 525 2.9.3 *The North Wyke Farm Platform*

526 The North Wyke Farm Platform, near Okehampton, SW England was established as a UK  
527 National Capability for collaborative research, training and knowledge exchange in agro-  
528 environmental sciences related to beef and sheep production in lowland grasslands (Orr et al.,  
529 2016). The soils on the farm platform are predominately Halstow, (Pelo-stagnogley soils,  
530 Avery, 1980), FAO Classification: Stagni-vertic cambisol, U.S. Soil Taxonomy: Typic  
531 haplaquept. For more details see Harrod and Hogan (2008). A system based on permanent  
532 pasture was implemented on three 21-ha farmlets to obtain baseline data on hydrology, nutrient  
533 cycling and productivity for 2 years. Since then, two of the farmlets have been modified by  
534 either (i) planned reseeded with grasses that have been bred for enhanced sugar content or  
535 deep-rooting traits or (ii) sowing grass and legume mixtures to reduce nitrogen fertilizer inputs.  
536 The third farmlet continued under permanent pasture. The quantities of nutrients that enter,  
537 cycle within and leave the farmlets are recorded using sensor technologies alongside more  
538 traditional field study methods. Here we simulated the water and nutrient flows from October  
539 2012 to 25<sup>th</sup> December 2013 from catchment 4 (Golden Rove) and catchment 5 (Orchard  
540 Dean), two of the un-modified permanent grassland catchments, that had contrasting  
541 topologies. The North Wyke data that we used for this study are available from  
542 <http://www.rothamsted.ac.uk/farmplatform>).

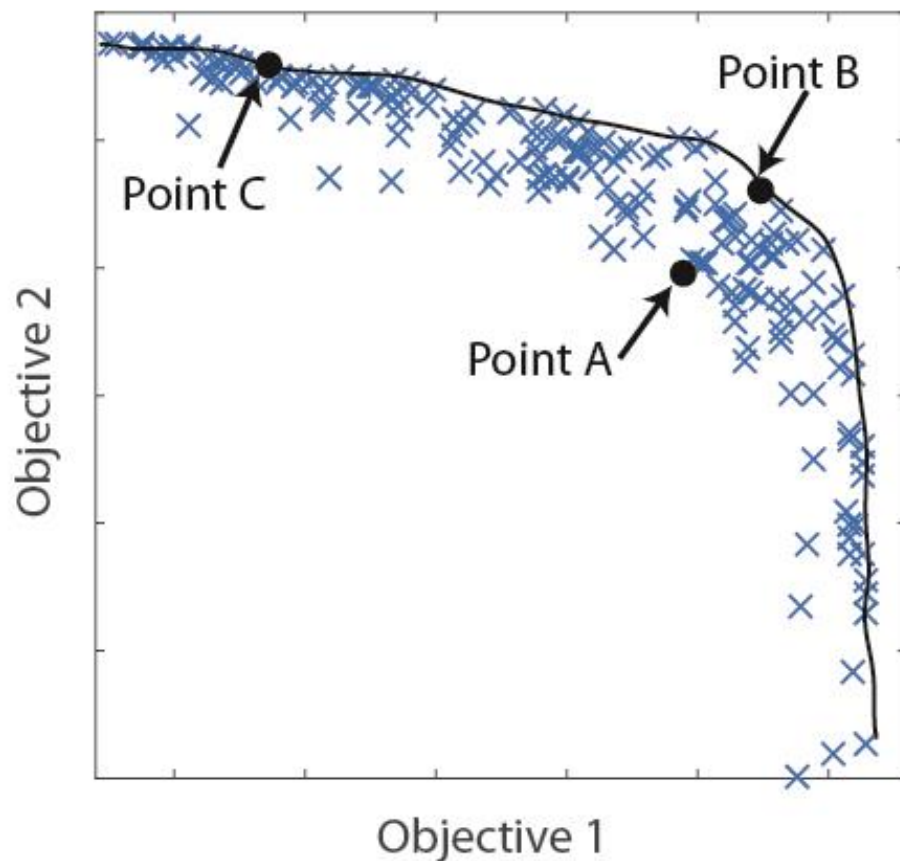
543

### 544 2.10 *Trade offs*

545 We coupled the simulation model with an optimisation algorithm to determine Pareto  
546 optimal fronts between multiple objectives defined in terms of outputs from the model. The  
547 optimised Pareto fronts describe the trade-offs between objective variables such as yield and

548 nitrate leaching. To illustrate how these can be identified, we used the fertiliser application  
549 time and amount as two management variables that the optimisation algorithm could vary in  
550 order to affect three objectives: the yield of a wheat crop, nitrate leaching and N<sub>2</sub>O emissions.  
551 Simulations used the soil properties and weather data from plot 9 of the Broadbalk experiment  
552 for the years 1968–1978. For this period the mean measured yield was 5.4 t ha<sup>-1</sup> at 85% dry  
553 matter.

554         Initially the algorithm, which combines non-dominated sorting (Deb et al., 2002) with  
555 differential evolution (Storn and Price, 1997), randomly selects a number of possible  
556 management variables, implements these management options in the simulation model and  
557 records the effect on each of the multiple objectives. Non-dominated sorting then identifies the  
558 management options that result in the ‘best’ objectives, i.e. those that are non-dominated. A  
559 point is said to be dominated by another if it is worse for every single objective. For example,  
560 if we aim to maximise two objectives, point A (Fig. 2) is dominated by point B because the  
561 value of both objectives is greater at B than A. Points B and C, however, are both non-  
562 dominated with respect to one another because whilst objective 1 is higher for B, objective 2  
563 is higher for C. The non-dominated sorting algorithm performs a series of pairwise  
564 comparisons in order to identify all of the management options that lead to non-dominated sets  
565 of objectives. The differential evolution algorithm then combines aspects of the management  
566 options that led to non-dominated objectives to identify new management options that could  
567 potentially perform even better. The process is iterated in directions that the differential  
568 evolution algorithm suggests will be an improvement, , until the results converge and produce  
569 a similar Pareto front with each iteration.



570

571 Fig.2 Example of how a Pareto front is identified from a number of points simulated by the  
 572 model with the aim to improve multiple objectives (1 & 2) simultaneously. Point B is selected  
 573 over point A because B scores better for both objectives. It can be seen that neither of points B  
 574 or C dominates the other, because point B does better at objective 1 whilst point C improves  
 575 on objective 2. Consequently, both are retained. The Pareto front (line) can be identified by  
 576 connecting together all of the non-dominated points.

577

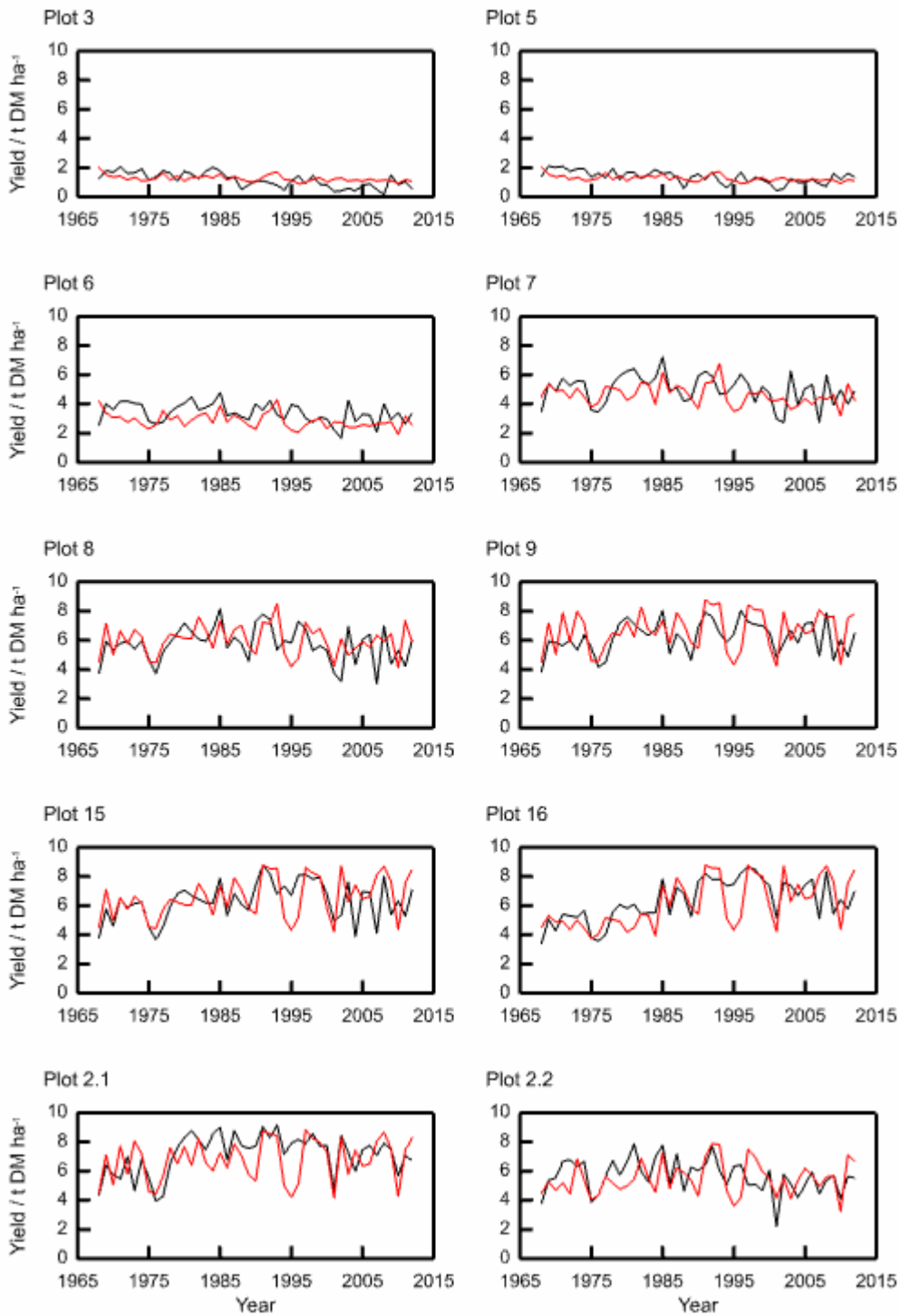
### 578 3. Results

#### 579 3.1 Broadbalk

580 The simulated and measured grain yields for the plots listed in Table 1 are shown in  
 581 Fig. 3. The model captures the differences between the plots well and this is quantified by the

582 overall correlation between modelled and measured (Pearson correlation,  $r = 0.86$ ). The plot  
583 means for the modelled and measured yields are similar, as are the variances, although the  
584 variance for the modelled yield in plots with little fertilizer N applied are smaller than the  
585 observed (Table 2). The model reflects the year-to-year fluctuations in yield, although notably  
586 under-predicts the 1995 yield from the plots with larger N applications (9, 15, 16, 2.1 and 2.2).

587



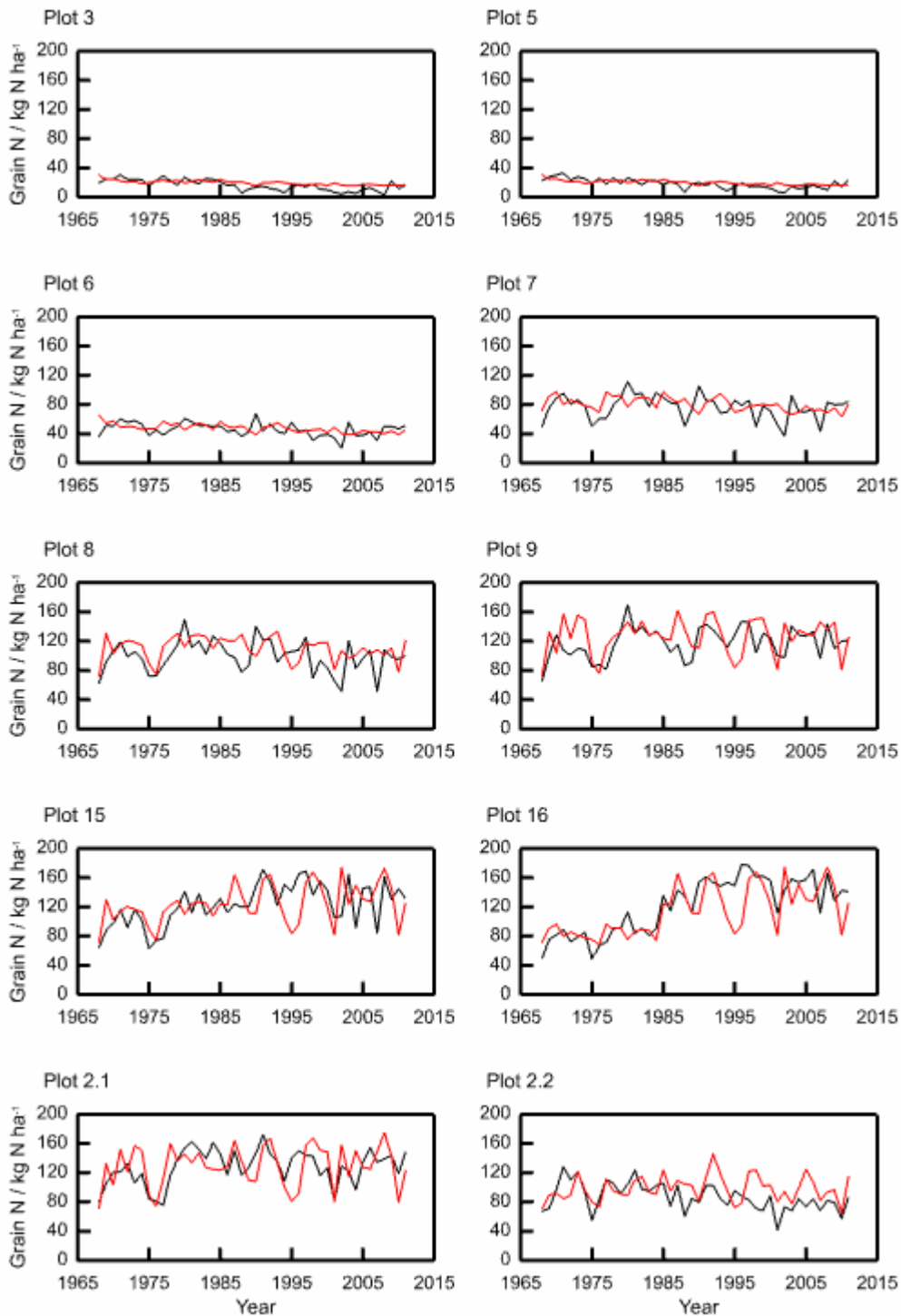
588

589 Fig. 3 Measured (black) and modelled (red) grain yields for ten plots from the Broadbalk  
 590 long-term wheat experiment, 1968-2012, continuous wheat (sections 1 and 9). The measured  
 591 values were averaged over Sections 1 and 9 (see 2.9.1).

592



593           The model replicates the plot-to-plot and year-to-year variation in grain N, grain P and  
594 TOC (see Figs 4, 3 and 6, and Tables 3, 4 and 5), although we note that year-to-year variation  
595 in TOC is minimal. The correlations across all plots between modelled and measured grain N,  
596 grain P, and TOC are 0.88, 0.84 and 0.99 respectively. The model reproduces the pattern in the  
597 variation of volumetric water content for plot 8, following one of the observed realisations  
598 closely (Fig. 7). Note that measurements with such probes are sometimes biased towards drier  
599 measurements because instrument range is short and if contact is lost between the access tube  
600 and soil then the soil can appear drier than it actually is.

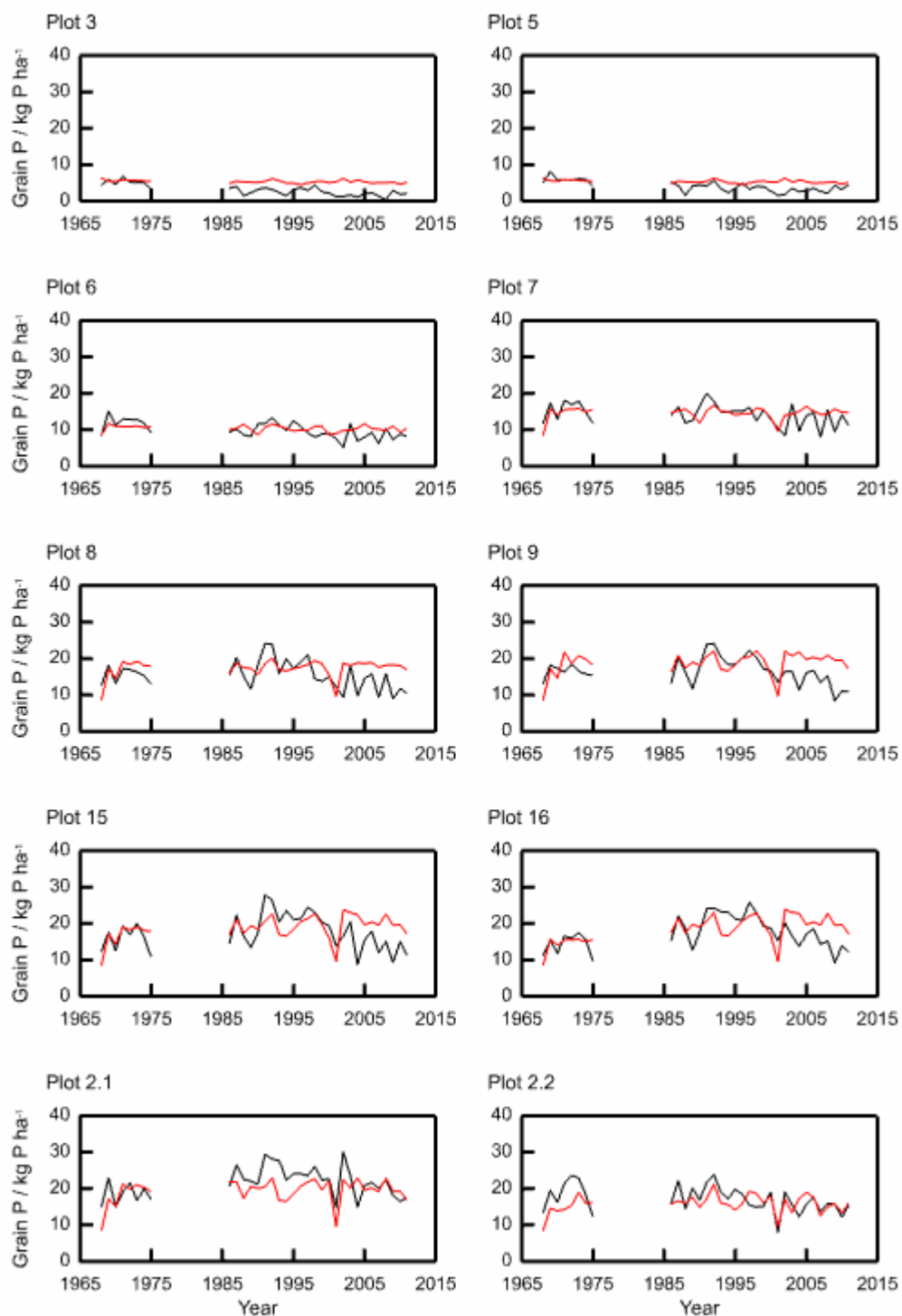


601

602 Fig. 4: Measured (black) and modelled (red) grain N content for ten plots from the Broadbalk  
 603 long-term wheat experiment, 1968-2012, continuous wheat. The measured values were from  
 604 Section 1 only (see 2.9.1).

605

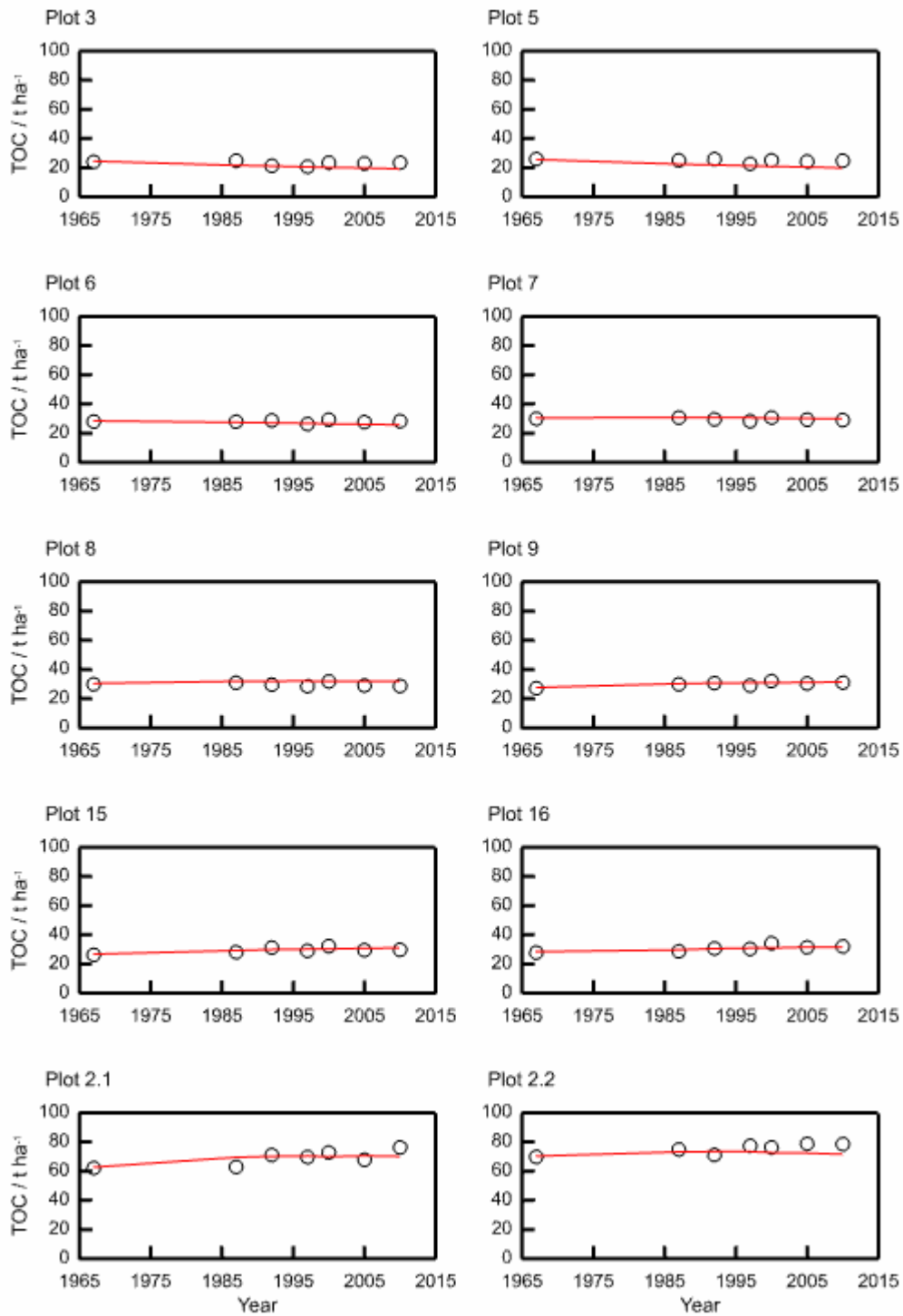
606



607

608 Fig. 5: Measured (black) and modelled (red) grain P content for ten plots from the Broadbalk  
 609 long-term wheat experiment (1968–1975 and 1986–2011), continuous wheat. The measured  
 610 values were from Section 1 only (see 2.9.1)

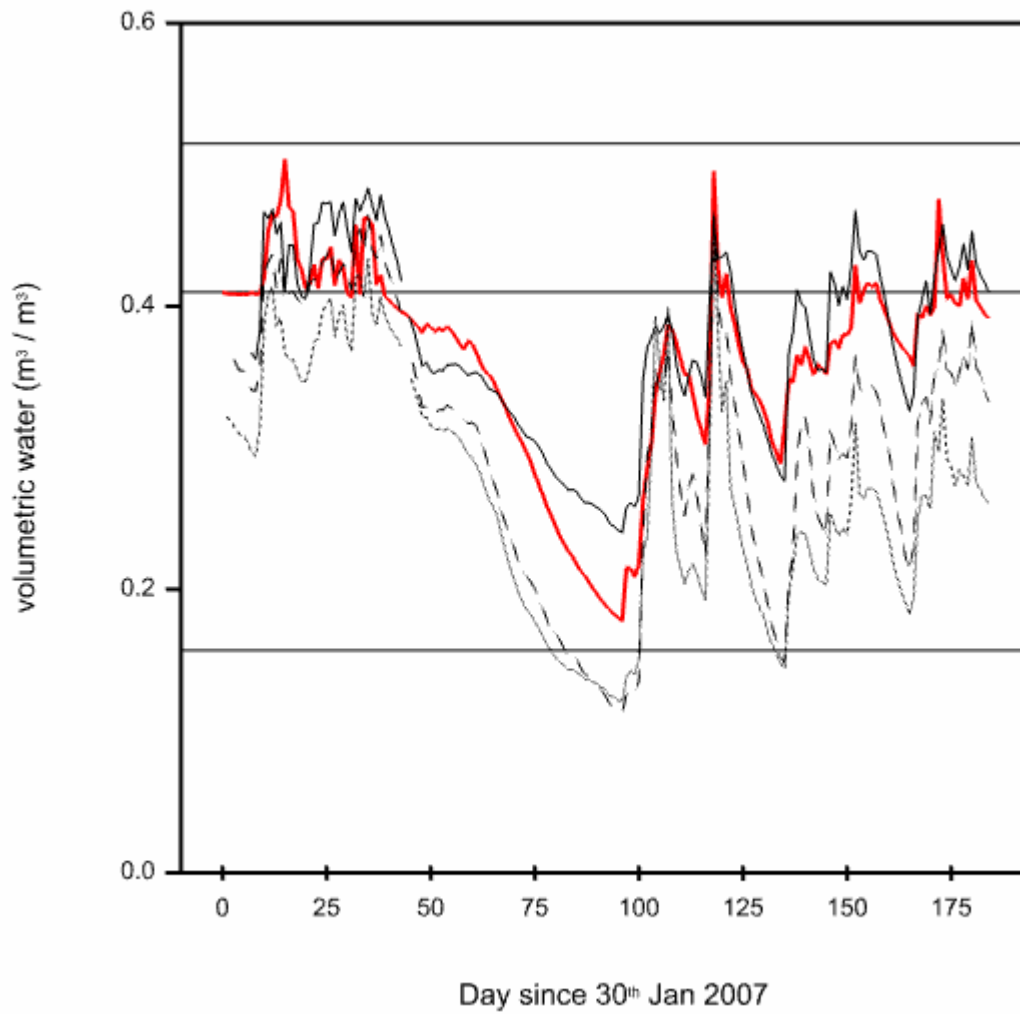
611



612

613 Fig. 6: Measured (black circles) and modelled (red) soil total organic carbon (TOC) for ten  
 614 plots from the Broadbalk long-term wheat experiment. The measured values were averaged  
 615 over Sections 1 and 9.

616



617

618 Fig. 7: Measured for three replicates (black) and modelled (red) volumetric water content in  
619 soil from plot 8 of the Broadbalk experiment.

620

621

622 Table 2 Summary statistics for measured and simulated grain yields (at 85% dry matter),  
 623 19682012 for the Broadbalk wheat experiment. The measured values for yield in each year  
 624 were averaged over Sections 1 and 9 (see 2.9.1).

Plot no.	Measured		Simulated		RMSE (%)	Correlation
	Mean t ha <sup>-1</sup>	Standard deviation/ t ha <sup>-1</sup>	Mean t ha <sup>-1</sup>	Standard deviation/ t ha <sup>-1</sup>		
3	1.16	0.5	1.26	0.22	42.56	0.28
5	1.37	0.42	1.27	0.22	33.41	0.16
6	3.4	0.67	2.86	0.51	28.61	0.07
7	4.99	1.02	4.62	0.7	24.03	0.16
8	5.71	1.18	6	1.01	24.27	0.25
9	6.23	1.06	6.66	1.32	23.01	0.36
15	6.32	1.28	6.58	1.37	23.29	0.4
16	6.34	1.41	6.12	1.64	20.88	0.64
2.1	7.16	1.35	6.75	1.41	20.28	0.49
2.2	5.67	1.12	5.49	1.13	22.84	0.35

625

626

627 Table 3 Summary statistics for measured and simulated grain N content, 1968–2012, for the  
 628 Broadbalk wheat experiment. The measured values for grain N were from Section 1 only (see  
 629 2.9.1).

630

Plot no.	Measured		Simulated		RMSE (%)	Correlation
	Mean kg N ha <sup>-1</sup>	Standard deviation/ kg N ha <sup>-1</sup>	Mean kg N ha <sup>-1</sup>	Standard deviation/ kg N ha <sup>-1</sup>		
3	16.33	7.23	19.76	3.1	42.54	0.57
5	18.48	6.36	20.07	3.15	31.58	0.47
6	46	9.12	47.69	5.79	23.42	0.03
7	76.69	16.21	80.44	9.03	23.58	0.11
8	99.03	21.31	110.25	15.84	25.44	0.29
9	117.91	20.91	126.27	23.92	23.32	0.32
15	122.99	28.03	124.05	25.96	25.17	0.35
16	121.34	37.12	113.62	32.82	22.98	0.71
2.1	128.08	23.56	129.28	27.52	21.27	0.44
2.2	86.83	18.58	98.09	17.27	27.04	0.34

631

632

633 Table 4 Summary statistics for measured and simulated P in the grain, 1968–1975 and 1986–  
 634 2011 for the Broadbalk wheat experiment. The measured values for grain P were from  
 635 Section 1 only (see 2.9.1).

636

Plot no.	Measured		Simulated		RMSE (%)	Correlation
	Mean kg P ha <sup>-1</sup>	Standard deviation/ kg P ha <sup>-1</sup>	Mean kg P ha <sup>-1</sup>	Standard deviation/ kg P ha <sup>-1</sup>		
3	3.04	1.49	5.36	0.43	89.47	0.29
5	4.05	1.47	5.4	0.43	48.33	0.26
6	9.89	2.23	10.35	0.86	22.5	0.26
7	14.11	2.89	14.58	1.66	20.73	0.29
8	15.38	3.85	17.31	2.38	29.01	0.23
9	16.49	3.59	18.64	3.06	27.8	0.26
15	17.47	4.73	18.77	3.27	28.34	0.33
16	17.33	4.3	18.42	3.57	25.47	0.42
2.1	21.49	4.09	19.36	3.26	20.42	0.47
2.2	17.14	3.57	15.8	2.5	20.24	0.49

637

638



639 Table 5 Summary statistics for measured and simulated total soil organic carbon (TOC),  
 640 when measured between 1967–2012 Broadbalk wheat experiment. The measured values for  
 641 TOC were averaged over Sections 1 and 9 (see 2.9.1).

642

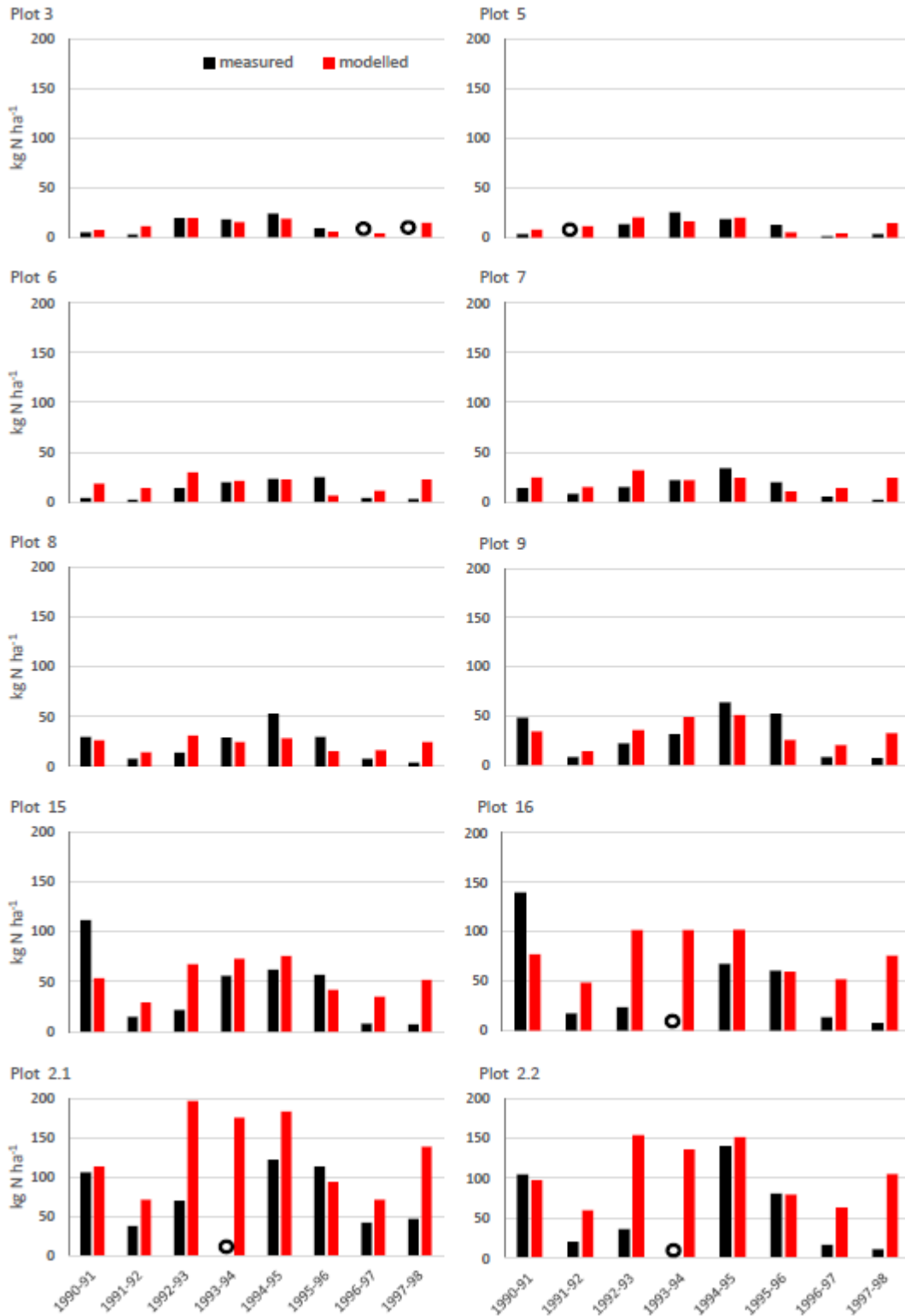
	<b>Measured</b>		<b>Simulated</b>			
<b>Plot no.</b>	Mean t C ha <sup>-1</sup> <sup>1</sup>	Standard deviation/ t C ha <sup>-1</sup>	Mean t C ha <sup>-1</sup>	Standard deviation/ t C ha <sup>-1</sup>	RMSE (%)	Correlation
3	22.95	1.37	21.01	1.6	11.51	0.28
5	24.84	1.05	21.78	1.76	13.83	0.47
6	27.96	0.88	26.82	0.84	6.07	-0.08
7	29.57	0.83	30.39	0.3	3.88	0.24
8	29.73	1.12	31.69	0.53	7.88	-0.1
9	29.97	1.47	30.36	1.18	3.11	0.82
15	29.45	1.84	29.74	1.33	4.42	0.72
16	30.75	1.96	30.55	1.06	4.3	0.78
2.1	68.9	4.76	68.97	2.61	5.46	0.62
2.2	75.18	3.27	72.36	1.06	5.61	0.28

643

644

645           The measured (Goulding et al., 2000) and modelled N leached for each plots are shown  
646 in Fig. 8. The model predictions match the N leached from the mineral fertilized plots  
647 reasonably well, although the model consistently overestimates N leached from plots receiving  
648 the most N (plots 15 and 16 and the FYM plots 2.1 and 2.2) and in the driest years (1991/2,  
649 1996/7 and 1997/8). The variances for measured leaching are larger than the modelled for all  
650 but plot 2.1 (Table 6). Note that measurements were not determined for every plot in every  
651 year.

652



653

654 Fig. 8: Estimated and modelled N leached from study plots on the Broadbalk wheat experiment

655 1990–1998. Measurements are from Section 9 only. The black open circle indicates that no

656 measurement was taken.

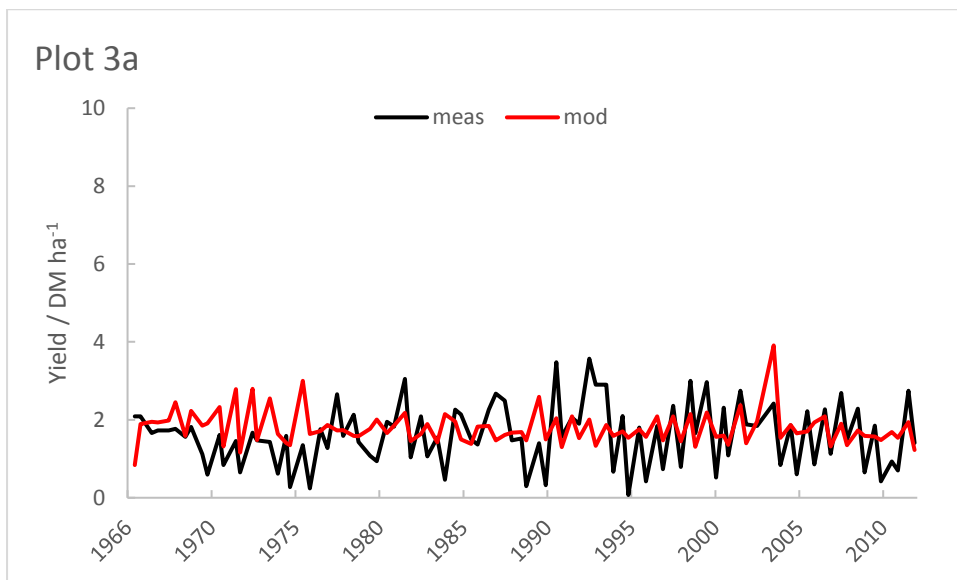
657 Table 6 Summary statistics for measured and simulated nitrate leached ( $\text{kg N ha}^{-1} \text{y}^{-1}$ ) between  
 658 1990 and 1998, Broadbalk wheat experiment. Measurements are from Section 9 only.

Plot no.	Measured		Simulated		RMSE (%)	Correlation
	Mean $\text{kg N ha}^{-1} \text{y}^{-1}$	Standard deviation/ $\text{kg N ha}^{-1} \text{y}^{-1}$	Mean $\text{kg N ha}^{-1} \text{y}^{-1}$	Standard deviation/ $\text{kg N ha}^{-1} \text{y}^{-1}$		
3	13.00	8.51	11.94	5.99	33.29	0.85
5	11.71	8.92	12.86	6.21	58.56	0.60
6	11.88	9.76	18.24	7.38	111.01	-0.02
7	15.00	10.38	20.68	7.01	81.13	0.17
8	22.00	16.55	22.73	6.47	65.70	0.36
9	30.00	22.44	32.74	12.83	57.82	0.58
15	42.38	33.31	53.57	17.51	79.79	0.36
16	47.57	47.02	77.51	22.69	107.32	0.23
2.1	76.86	36.19	130.33	50.46	85.84	0.38
2.2	59.00	50.10	105.98	37.58	103.82	0.45

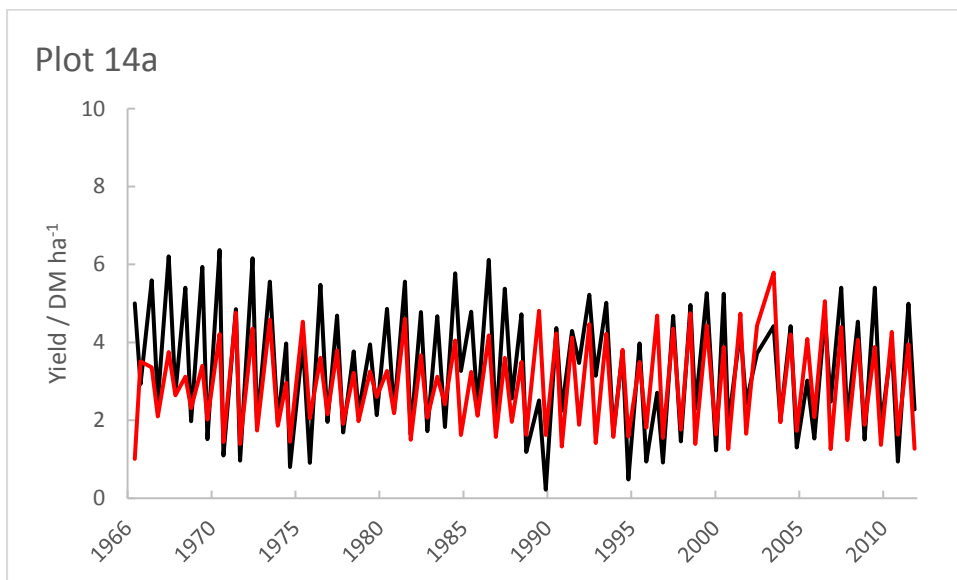
659

660 3.2 Park Grass

661 The model captures the differences between the plots and between the first and second cuts  
662 well (Figure 9 and Table 7). The first cut, usually taken in June, is normally higher than the  
663 second cut which is usually taken in November).



664  
665



666  
667

668 Figure 9 Simulated (red) and measured (black) yields for plots 3a and 14/2a Park Grass  
669 permanent grassland experiment, showing both cuts each year.

670 Table 7 Summary statistics for measured and simulated yield 1966-2012, Park Grass  
 671 experiment, (47 years, n = 93).

	<b>Measured</b>		<b>Simulated</b>			
<b>Plot no.</b>	Mean t ha <sup>-1</sup>	Standard deviation/ t ha <sup>-1</sup>	Mean t ha <sup>-1</sup>	Standard deviation/ t ha <sup>-1</sup>	RMSE (%)	Correlation
3a	1.61	0.78	1.79	0.43	49.91	0.28
14/2a	3.32	1.67	2.91	1.24	34.35	0.77

672

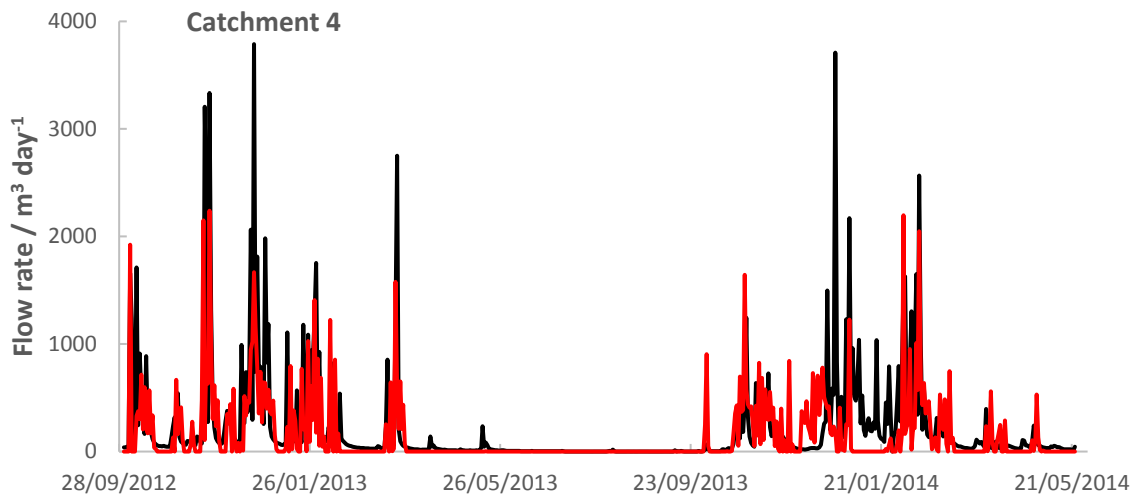
673

### 674 3.2 North Wyke Farm Platform

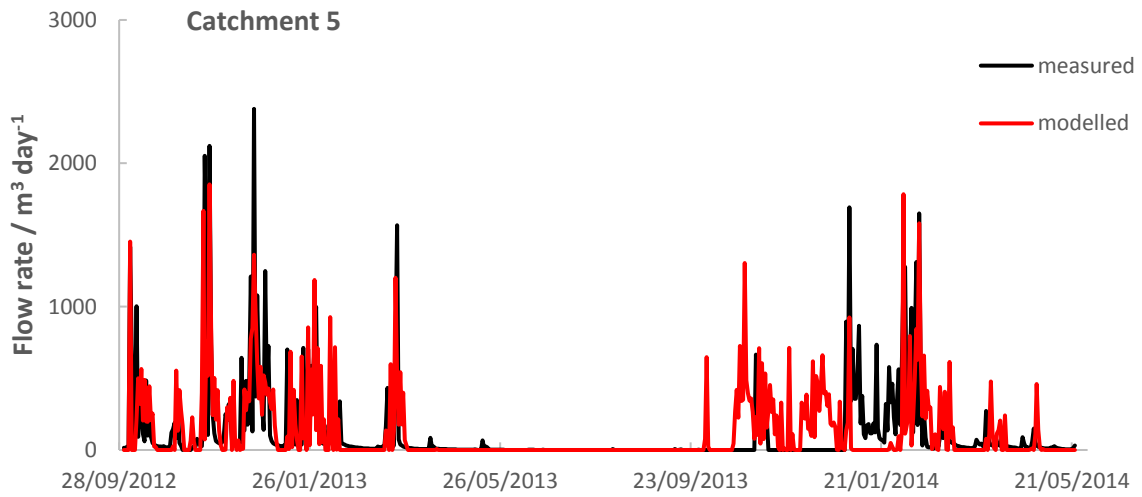
675 The simulation of water flow rates (m<sup>3</sup> day<sup>-1</sup>) for catchments 4 and 5 reflect those measured  
 676 (Fig. 10 and Table 8). This is quantified by the correlations between modelled and measured  
 677 (Pearson correlation,  $r = 0.57$  and  $r = 0.55$  respectively). The modelled water flow rate and  
 678 variation are slightly smaller than the measured in each case.

679

680



681



682

683 Fig. 10 Simulated (red) and measured (black) flow rates ( $\text{m}^3 \text{day}^{-1}$ ) for catchment 4 and 5 of  
684 the North Wyke Farm Platform

685

686

687 Table 8 Summary statistics for measured and simulated flow and nitrate (kg N per catchment per day) in the drains, North Wyke Farm Platform

688 Catchments 4 and 5.

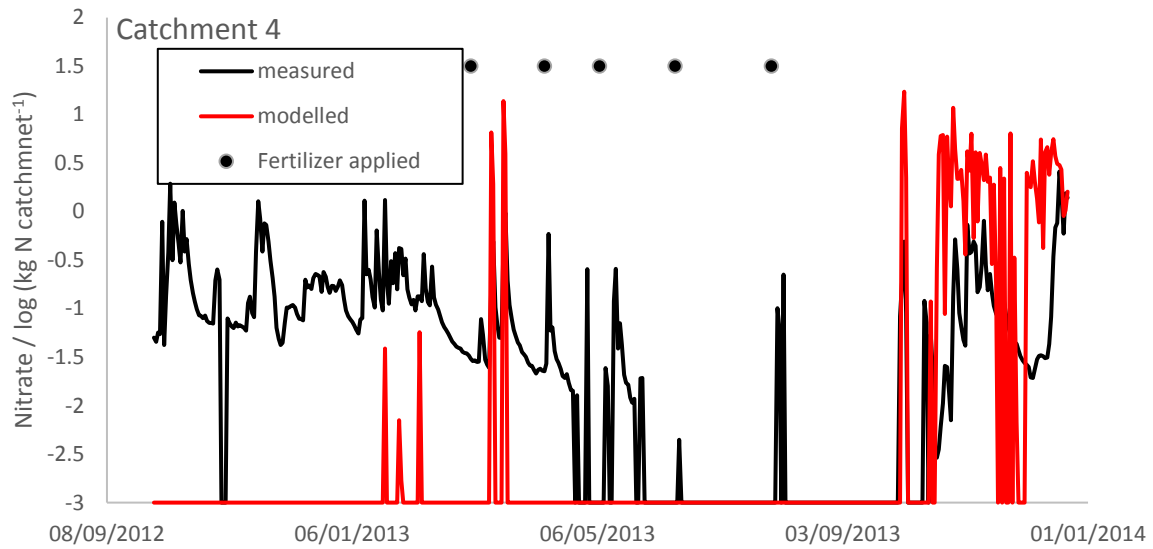
	Flow (m <sup>3</sup> day <sup>-1</sup> )						Nitrate (kg N catchment <sup>-1</sup> day <sup>-1</sup> )					
	Measured		Simulated		RMSE (%)	Correlation	Measured		Simulated		RMSE (%)	Correlation
Catchment	Mean	Std dev	Mean	Std dev			Mean	Std dev	Mean	Std dev		
4	213.60	457.01	147.83	315.90	180.36	0.57	0.13	0.27	0.47	1.64	1287.69	0.21
5	114.10	281.82	122.88	258.19	226.02	0.55	0.13	0.29	0.01	0.08	248.45	-0.01

689

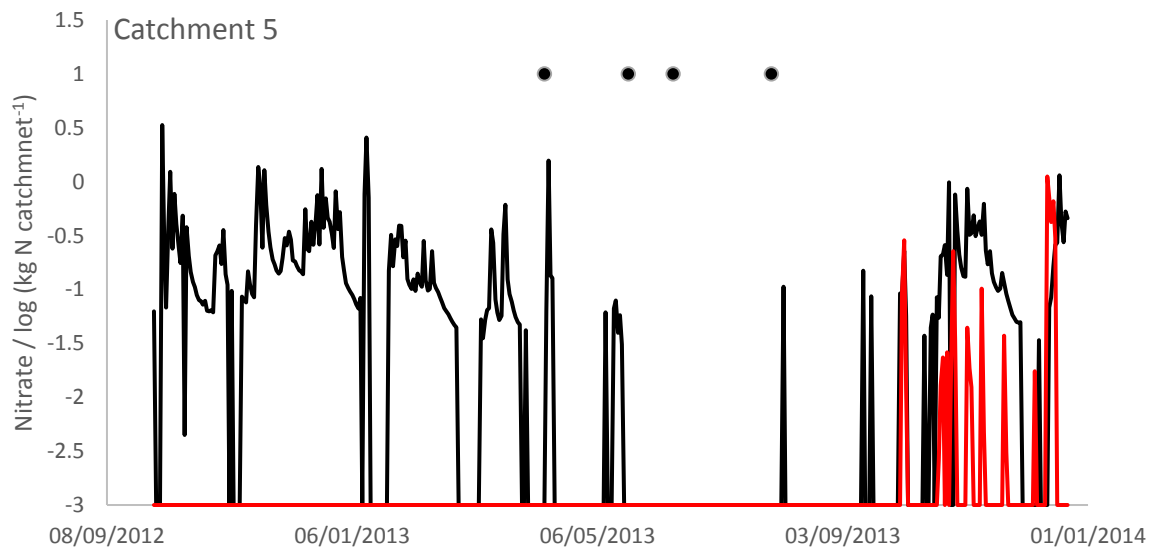
690



691 The simulation of nitrate in the drainage water over estimates nitrate for catchment 4  
 692 and under estimates it for catchment 5, but the peaks of nitrate after May 2013 broadly  
 693 correspond to that which was measured (see Fig. 11 and Table 8).



694



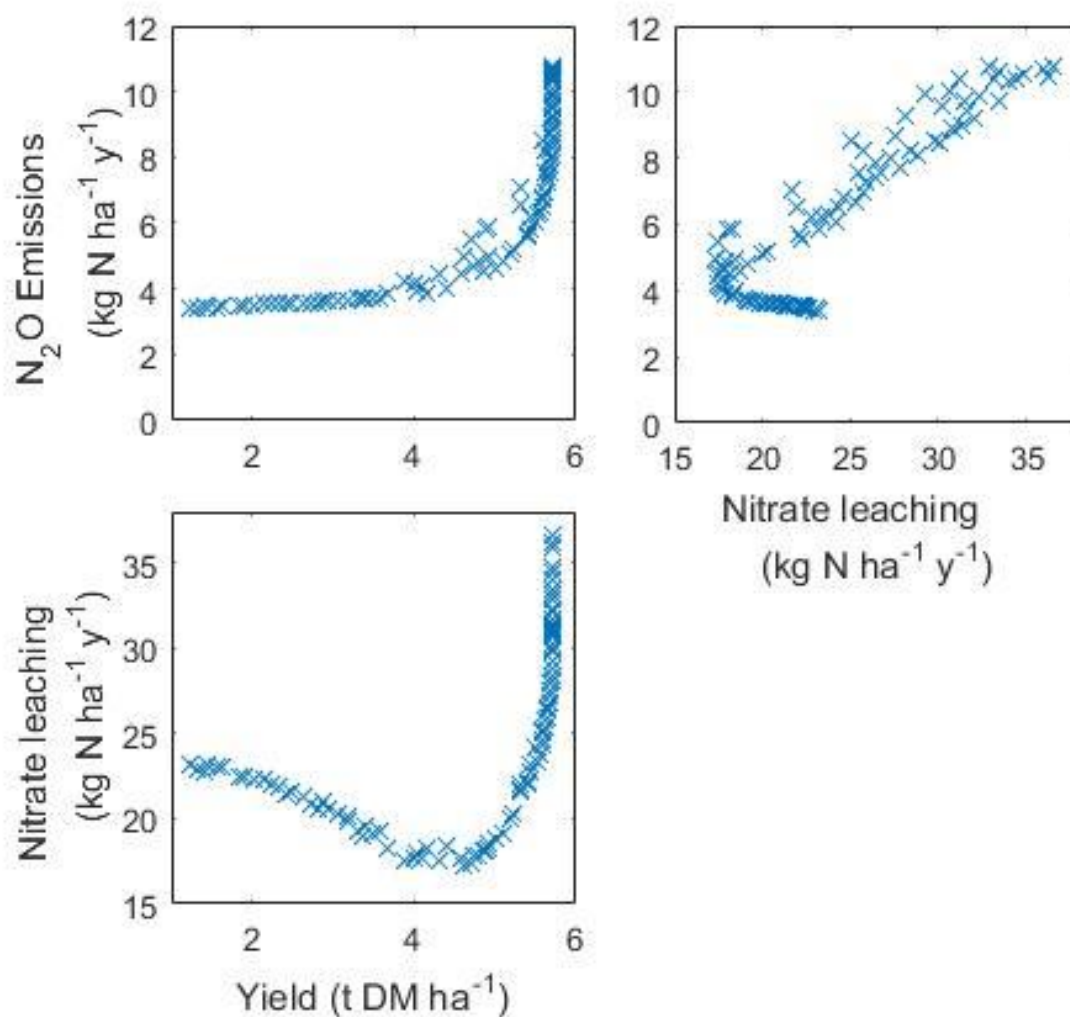
695

696 Fig. 11 Simulated (red line) and measured (black line) log nitrate (kg N /catchment) for  
 697 catchment 4 and 5 of the North Wyke Farm Platform. The black discs show when nitrogen  
 698 fertilizer was applied. For details see <http://www.rothamsted.ac.uk/farmplatform>.

699

### 700 3.3 Trade offs

701 By allowing an optimisation algorithm to vary the timing and amount of a single fertilizer  
702 application, we identified the trade-offs between yield, nitrate leaching and N<sub>2</sub>O emissions for  
703 an illustrative example (Fig. 12). The results show that as the yield increases (due to changes  
704 in fertilizer application) the lowest possible N<sub>2</sub>O emissions that could be achieved  
705 simultaneously increases non-linearly. The range of fertilizer N applied to achieve these Pareto  
706 optimal objectives was 0 – 210 kg N ha<sup>-1</sup> y<sup>-1</sup>. The N<sub>2</sub>O emissions reduce as a result of applying  
707 less fertilizer later in the growing season. As yield approaches its maximum, both the N<sub>2</sub>O  
708 emissions and the nitrate leaching increase substantially with increasing amounts of fertilizer  
709 for an increasingly marginal improvement in yield. Nitrate leaching and N<sub>2</sub>O emissions are  
710 synergistic throughout most of the range, however a trade-off appears as the emissions reach  
711 their minimum value, as this also results in an increase in leaching. This illustrates how an  
712 optimisation approach (e.g. minimising N<sub>2</sub>O) could have unintended consequences for another  
713 process (nitrate leaching), if both objectives are not considered simultaneously. The  
714 optimisation algorithm does not identify a single fertilisation strategy, but highlights  
715 nonlinearities thus identifying where a small reduction in one objective could have a large  
716 benefit to another. Here, for example, the simulation indicates that the fertilizer application  
717 conditions which correspond to a moderate yield, reduce the nitrate that is available to leach  
718 from the soil substantially compared to those required for the most yield.



719

720

721 Fig. 12 Illustrative example of use of the model to identify trade-offs between multiple  
 722 objectives such as maximising yield, minimising nitrate leaching and minimising  $N_2O$   
 723 emissions. As maximising or minimising any one of these objectives affects the others, the  
 724 optimisation identifies points on a multi-dimensional frontier with Pareto optimality. On this  
 725 frontier no objective can be improved upon without a detrimental effect on at least one of the  
 726 other objectives. This frontier therefore represents the best trade-offs that can be achieved.

727

728

#### 729 4. Discussion

730 We have built and used a model framework to simulate spatial and temporal interactions  
731 in agricultural landscapes. The framework allows us to explore trade-offs between production  
732 and environmental outcomes to determine strategies that could contribute to sustainable food  
733 production. It is important that the models reflect the important mechanisms that relate to  
734 production and the environment. It is also essential that the models are parsimonious and run  
735 quickly so that a large range of scenarios can be tested, perhaps in conjunction with an  
736 optimisation algorithm. Our simulations are within 25% of all the observations across multiple  
737 years and plots and this is good evidence that the model is robust and that we can use it with  
738 confidence to explore trade-offs relevant to farm and environmental management.

739 Simulation of wheat yields from the Broadbalk experiment and grass yields from the  
740 Park Grass experiment reproduced both the differences between plots caused by the various  
741 fertilizer rates ( $\rho > 0.78$ ) and the observed year-to-year variation (RMSE ranging between  
742 20.3 and 28.6% for the mineral N and FYM plots on Broadbalk and 34.3% for Park Grass,  
743 correlations were up to 0.77). According to the RMSEs, the model performed less well for the  
744 plots that received no fertilizer (plots 3 and 5 on Broadbalk and plot 3a on Park Grass) where  
745 the RMSEs were 42.6, 33.4% and 49.9% respectively. The larger values for the RMSE on the  
746 lower-yield plots to some extent result from the form of this statistic which is scaled by the  
747 reciprocal of the mean observation (i.e. the sum of the squared difference for the lower-yielding  
748 plots are scaled by larger values than the higheryielding plots). Over the 46 years that we  
749 simulated Broadbalk, the model tended to under predict yield between 1994 and 1996 for plots  
750 with higher rates of N fertilizer applied (plots 8, 9, 15, 16, 21, 22) (Fig. 3). This is likely to be  
751 a result of excessive water stress when there was no N limitation. It was drier than normal in  
752 the three months before harvest in 1994, 1995 and 1996, this led to higher water stress during  
753 those months, and so a reduction in dry matter production.

754 The predictions of the variation in grain N for the Broadbalk plots were also good, with  
755 the RMSE ranging from 21.3 to 42.5% (Fig. 4, Table 3), and again illustrated the differences  
756 between plots receiving different rates of fertilizer N. For P uptake by the crop, the model  
757 performed well for most plots with RMSE between 20.2 – 29.0% for all plots except 3 and 5  
758 which had RMSE of 89.5% and 48.3% respectively (Fig. 5 and Table 4). In the experiment  
759 applications of P stopped in 2001 due to large amounts of plant-available P in the soil, and the  
760 P measured in the grain declines noticeably in plots with larger applications of fertilizer but  
761 this is not exhibited in the model. However, this does not affect the measured grain yields (Fig  
762 3). The variations in simulated yield, grain N and P are approximately 50% smaller than the  
763 observed for plots 3 and 5 (for other plots the variation is proportionally more similar). This  
764 suggests that the nitrogen stress function maybe over-damping the simulated response to  
765 variation in the weather.

766 The modelled total soil organic carbon for the Broadbalk plots fits the measured data  
767 well with the RMSE ranging from 3.1 to 13.8% (Fig. 6 and Table 5).

768 The model simulations of N leached from the Broadbalk plots were compared with  
769 estimates of leaching from (Goulding et al., 2000), based on nitrate concentrations in drainage  
770 and soil water and calculations of drain flow. The measured concentrations of nitrate in soil  
771 water were subject to the usual large spatial variation with typical CVs of 50–90%. The  
772 simulations reflected the differences in leaching between the different amounts of N, although  
773 they tended to overestimate N leached at the largest N rates and in the driest years (Fig. 8 and  
774 Table 6). IPCC guidelines (IPCC, 1997;Del Grosso et al., 2005) assume that 30% of applied N  
775 is leached or runs off into groundwater or surface waters and this accords with our simulations  
776 of Broadbalk where approximately 31.7% of N applied is lost through leaching.

777           The simulation of water flow from the two North Wyke Catchments matches the pattern  
778 in the variation of water flow but the average water flow over the simulated periods was larger  
779 than that simulated, as was the variation. This suggests that our model system is buffering the  
780 water through-put in the catchment and that too much is being taken by the crop or evaporating  
781 from the system. The simulations of nitrate in drainage water on the North Wyke plots appeared  
782 to be poorer than the simulations of N losses for Broadbalk. Although the timing of peaks in  
783 nitrate towards the end of the simulation were determined well, little nitrate was simulated in  
784 the first part of the simulated time period. This was because there was very little nitrate left in  
785 the model soil profiles at the beginning of the simulated run, and during the summer period  
786 (May 2013 – September 2013) there was very little simulated discharge (see Fig. 10). An  
787 addition of nitrate on 5<sup>th</sup> March 2013 to catchment 4 increased the nitrate levels in the soil and  
788 a peak in nitrate followed. Further additions of nitrate fertilizer kept the soil nitrate in this  
789 simulation at a larger concentration than that in the catchment 5 simulation, which despite  
790 having similar levels of nitrate applied, retained less nitrate in the soil. The difference in the  
791 simulated soil nitrate between the two catchments manifests as differences in the nitrate in the  
792 drainage water in the autumn and winter of 2013 where the nitrate leached was greater for  
793 catchment 4 than for catchment 5. The simulated nitrate in the drainage water is larger than  
794 that measured for catchment 4 yet smaller for catchment 5. This suggests problems with the  
795 modelled uptake of nitrate by the grass and retention in the soil in this case, but we have no  
796 explanation for the counter-intuitive discrepancy between the measurements on the two plots.  
797 Quantifying the fate of nitrate is notoriously difficult (Senapati et al., 2016). Recently  
798 calculated field level budgets of N from the North Wyke platform show unaccounted for losses  
799 of between 30 and 60 kg N ha<sup>-1</sup> (Misselbrook pers. comm.). This highlights the need for more  
800 research on the processes that control N transformations from micro-scale to field scale, and  
801 larger-scales. Facilities such as the North Wyke farm platform are ideally placed to support

802 this kinds of research. Models such as the one described here can help to identify the parts of  
803 the processes where understanding is incomplete and so can help to inform the design of  
804 experiments as well as benefit from any new understanding obtained.

805 Others have explored trade-offs using empirical data. For example Phalan et al. (2011)  
806 compared the effects of land sparing and land sharing on crop yields and the densities of tree  
807 and bird species across the UK, while Lamb et al. (2016) explored the need to cut greenhouse  
808 gas emissions, while increasing agricultural yields to meet the rapidly rising food demand  
809 through land sparing. Eory et al. (2013) examined the trade-offs and synergies between  
810 greenhouse gas mitigation measures and other environmental pollutants. The limitation of such  
811 empirical studies is that there is a lack of data and so it is often not possible to consider more  
812 than two factors at a time. Whilst models should always be used with caution, they do allow us  
813 to consider multiple interactions under a large range of management strategies. Used  
814 appropriately, models such as the one we present here should allow sound conclusions to be  
815 drawn on the relative impact of management strategies and might highlight unintended  
816 consequences of certain actions. Whilst the complexity of agricultural systems across the  
817 landscape could warrant a complex model, a simpler model that runs more quickly but still  
818 captures the key processes can be coupled more easily to an optimisation algorithm. This then  
819 provides the opportunity to identify the form of the synergies and trade-offs between multiple  
820 objectives at a broad and often neglected scale. Here, for example, we observe that objectives  
821 that are largely synergistic such as nitrate leaching and N<sub>2</sub>O emissions still exhibit a trade-off  
822 as the N<sub>2</sub>O emissions approach the minimum. The non-linearity in the leaching and emissions  
823 as yield increases is also clear, indicating a strong trade-off.

824 In order to generate frontiers such as the ones we did here (Fig. 12) an optimisation  
825 algorithm must be chosen and a set of management options that the optimisation algorithm can  
826 manipulate identified. Within an agricultural landscape, management options are numerous.

827 For example, even considering only fertiliser applications, the timing, amount and type of  
828 multiple applications could all be included in the set of management options to be optimised.  
829 This set of options will constrain the frontier, thus care must be taken to identify a reasonable  
830 range of options, whilst keeping the number of variables that the algorithm can manipulate to  
831 a minimum. Even so, the set of options is likely to represent a complex optimisation problem,  
832 involving multiple control variables, with the risk that the algorithm may be trapped in local  
833 minima. The optimisation algorithm must be chosen and implemented to minimise this risk. In  
834 this case we chose to use non-dominated sorting combined with differential evolution. Whilst  
835 the non-dominated sorting allowed us to consider multiple-objectives, which is critical to our  
836 aim of generating trade-off curves, the differential evolution combines a genetic algorithm and  
837 a gradient based search to allow a complex control space to be explored efficiently.

838 Our framework includes models of crop growth, the dynamics of soil conditions and  
839 water and nutrient flows in order to quantify the trade-offs between agricultural production and  
840 environmental factors. It could be expanded to include volatilisation and biological N fixation  
841 (which should improve the simulation for certain grass and crop types). Our framework is  
842 distinct from alternative models of the agricultural landscape because it simulates multiple  
843 functions simultaneously and distinct from other models of ecosystem services (e.g. Sharps et  
844 al., 2017) because it focuses on scaling up the effect of field and farm scale management  
845 practices to landscape scale. Additional environmental factors are also relevant to the  
846 agricultural landscape and to include these the model could be expanded to include weeds,  
847 pests and diseases and aspects of biodiversity. For each new component there will be feedbacks  
848 into existing models that alter the dynamics of yield accumulation and soil nutrient status. For  
849 example, weed population dynamics will depend on the crop and the soil conditions, but in turn  
850 weeds will have a competitive effect on the crop, primarily for light, that will affect both yield  
851 and to some extent soil nutrient status (Kropff and van Laar, 1993). Our model framework is



852 spatially explicit and simulates interactions between cells, in particular it describes the lateral  
853 flows of nutrients and water from cell to cell based on relative elevation and slope of model  
854 cell. The movement of insect pests, for example, is somewhat different as choice of destination  
855 are influenced by host plant distribution and the dispersal characteristics of the species in  
856 question. It will be straightforward to include these dispersal mechanisms within the landscape  
857 framework, see Milne et al. (2015).

858

### 859 **Acknowledgements**

860 This research was funded by the Biotechnology and Biological Sciences Research Council  
861 (BBSRC) Institute Strategic Programme grant Delivering Sustainable Systems (DSS) and  
862 BBSRC ISP Soils 2 Nutrition (S2N), using facilities funded by the BBSRC and also partly by  
863 NERC grant NE/J011568/1. We thank P J Gregory for providing root length data, Paul Pulton  
864 for soil P data, Jess Evans and Hadewij Sint for help with the North Wyke Farm Platform data,  
865 and Chris Watts for providing the soil moisture data. We thank the Lawes Agricultural Trust  
866 and Rothamsted Research for data from the e-RA database. The Rothamsted Long-term  
867 Experiments National Capability is supported by the BBSRC and the Lawes Agricultural  
868 Trust. The North Wyke Farm Platform is a UK National Capability supported by the  
869 Biotechnology and Biological Sciences Research Council (BBSRC BB/J004308/1).

870

871

### 872 **References**

873 Addiscott TM, Whitmore AP. Simulation of solute leaching in soils of differing permeabilities.  
874 Soil Use and Management 1991; 7: 94-102

875 Andam KS, Ferraro PJ, Pfaff A, Sanchez-Azofeifa GA, Robalino JA. Measuring the  
876 effectiveness of protected area networks in reducing deforestation. Proceedings of the  
877 National Academy of Sciences of the United States of America 2008; 105: 16089-  
878 16094, <http://dx.doi.org/10.1073/pnas.0800437105>

879 Andrew IKS, Storkey J. Using simulation models to investigate the cumulative effects of  
880 sowing rate, sowing date and cultivar choice on weed competition. Crop Protection  
881 2017; 95: 109-115, <http://dx.doi.org/10.1016/j.cropro.2016.05.002>

882 Anon. Sundial-FRS user guide, IACR-Rothamsted and MAFF, 1998, pp. 60

883 Avery BW. Soil classification for England and Wales (Higher categories). Soil Survey,  
884 Technical Monograph No. 14. Rothamsted Experimental Station, Harpenden, England  
885 1980, 10.1002/jpln.19811440221

886 Avery BW, Catt JA. The Soil at Rothamsted. Harpenden, Herts: Lawes Agricultural Trust,  
887 1995

888 Bell MJ, Jones E, Smith J, Smith P, Yeluripati J, Augustin J, et al. Simulation of soil nitrogen,  
889 nitrous oxide emissions and mitigation scenarios at 3 European cropland sites using the  
890 ECOSSE model. Nutrient Cycling in Agroecosystems 2012; 92: 161-181,  
891 10.1007/s10705-011-9479-4

892 Bell VA, Kay AL, Jones RG, Moore RJ. Development of a high resolution grid-based river  
893 flow model for use with regional climate model output. Hydrology and Earth System  
894 Sciences 2007; 11: 532-549

895 Boons-Prins ER, de Koning GHJ, van Diepen CA, Penning de Vries FWT. Crop-specific  
896 simulation parameters for yield forecasting across the European Community.  
897 Simulation Reports CARO-TT, cabo-dlo, 1993

898 Bouman BAM, Schapendonk AHCM, Stol W, van Kraalingen DWG. Description of the  
899 grassland growth model LINGRA as implemented in CGMS ab-dlo, 1996

900 Bradbury NJ, Whitmore AP, Hart PBS, Jenkinson DS. Modeling the Fate of Nitrogen in Crop  
901 and Soil in the Years Following Application of N-15-Labeled Fertilizer to Winter-  
902 Wheat. *Journal of Agricultural Science* 1993; 121: 363-379

903 Brisson N, Gary C, Justes E, Roche R, Mary B, Ripoche D, et al. An overview of the crop  
904 model STICS. *European Journal of Agronomy* 2003; 18: 309-332,  
905 [http://dx.doi.org/10.1016/s1161-0301\(02\)00110-7](http://dx.doi.org/10.1016/s1161-0301(02)00110-7)

906 Colbourn P. The influence of drainage and cultivation on denitrification losses from an arable  
907 clay soil. In: Jenkinson DS, Smith KA, editors. *Nitrogen Efficiency in Agricultural*  
908 *Soils*. Elsevier Applied Science, England, 1988, pp. 283-294

909 Coleman K, Jenkinson DS. RothC - A Model for the turnover of carbon in soil: Model  
910 description and users guide (updated June 2014). Harpenden, UK: Lawes Agricultural  
911 Trust, 2014

912 Coleman K, Jenkinson DS, Crocker GJ, Grace PR, Klir J, Korschens M, et al. Simulating trends  
913 in soil organic carbon in long-term experiments using RothC-26.3. *Geoderma* 1997; 81:  
914 29-44

915 Cottrill BR, Smith KA. Nitrogen output of livestock excreta. Final report, Defra Project  
916 WT0715NVZ, DEFRA, 2007

917 Deb K, Pratap A, Agarwal S, Meyarivan T. A fast and elitist multiobjective genetic algorithm:  
918 NSGA-II. *Ieee Transactions on Evolutionary Computation* 2002; 6: 182-197,  
919 <http://dx.doi.org/10.1109/4235.996017>

920 Del Grosso SJ, Mosier AR, Parton WJ, Ojima DS. DAYCENT model analysis of past and  
921 contemporary soil N(2)O and net greenhouse gas flux for major crops in the USA. *Soil*  
922 *& Tillage Research* 2005; 83: 9-24, <http://dx.doi.org/10.1016/j.still.2005.02.007>

923 Del Grosso SJ, Parton WJ, Mosier AR, Ojima DS, Kulmala AE, Phongpan S. General model  
924 for N<sub>2</sub>O and N<sub>2</sub> gas emissions from soils due to denitrification. *Global Biogeochemical*  
925 *Cycles* 2000; 14: 1045-1060

926 Del Prado A, Misselbrook T, Chadwick D, Hopkins A, Dewhurst RJ, Davison P, et al.  
927 SIMSDAIRY: A modelling framework to identify sustainable dairy farms in the UK.  
928 Framework description and test for organic systems and N fertiliser optimisation.  
929 *Science of the Total Environment* 2011; 409: 3993-4009,  
930 <http://dx.doi.org/10.1016/j.scitotenv.2011.05.050>

931 Eory V, Topp CFE, Moran D. Multiple-pollutant cost-effectiveness of greenhouse gas  
932 mitigation measures in the UK agriculture. *Environmental Science & Policy* 2013; 27:  
933 55-67, <http://dx.doi.org/10.1016/j.envsci.2012.11.003>

934 Feddes RA, Kowalik P, Kolinskamalinka K, Zaradny H. Simulation of field water-uptake by  
935 plants using a soil-water dependent root extraction function. *Journal of Hydrology*  
936 1976; 31: 13-26, [http://dx.doi.org/10.1016/0022-1694\(76\)90017-2](http://dx.doi.org/10.1016/0022-1694(76)90017-2)

937 Gerwitz A, Page ER. An empirical mathematical model to describe plant root systems. *Journal*  
938 *of Applied Ecology* 1974; 11: 773–781

939 Gil JDB, Reidsma P, Giller KE, Todman LC, Van Ittersum MK. Agriculture, food security and  
940 the Sustainable Development Goals: theory and practice in three development contexts.  
941 *Global Environmental Change (submitted)* 2017

942 Godwin DC, Allan Jones C. Nitrogen dynamics in soil-plant systems. Modeling plant and soil  
943 systems. ASA-CSSA-SSSA, Madison, 1991

944 Goulding KWT, Poulton PR, Webster CP, Howe MT. Nitrate leaching from the Broadbalk  
945 Wheat Experiment, Rothamsted, UK, as influenced by fertilizer and manure inputs and  
946 the weather. *Soil Use and Management* 2000; 16: 244-250

947 Harrod TR, Hogan DV. The Soil of North Wyke and Rowden: North Wyke Research, North  
948 Wyke, Devon, 2008

949 IPCC. Intergovernmental panel on climate change guidelines for national greenhouse gas  
950 inventories. Agriculture: Nitrous Oxide from Agricultural Soils and Manure  
951 Management. OECD, Paris, 1997

952 Jackson B, Pagella T, Sinclair F, Orellana B, Henshaw A, Reynolds B, et al. Polyscape: A GIS  
953 mapping framework providing efficient and spatially explicit landscape-scale valuation  
954 of multiple ecosystem services. Landscape and Urban Planning 2013; 112: 74-88,  
955 <http://dx.doi.org/10.1016/j.landurbplan.2012.12.014>

956 Keating BA, Carberry PS, Hammer GL, Probert ME, Robertson MJ, Holzworth D, et al. An  
957 overview of APSIM, a model designed for farming systems simulation. European  
958 Journal of Agronomy 2003; 18: 267-288, [http://dx.doi.org/10.1016/s1161-](http://dx.doi.org/10.1016/s1161-0301(02)00108-9)  
959 [0301\(02\)00108-9](http://dx.doi.org/10.1016/s1161-0301(02)00108-9)

960 Koh LP, Lee TM, Sodhi NS, Ghazoul J. An overhaul of the species-area approach for  
961 predicting biodiversity loss: incorporating matrix and edge effects. Journal of Applied  
962 Ecology 2010; 47: 1063-1070, <http://dx.doi.org/10.1111/j.1365-2664.2010.01860.x>

963 Kropff MJ, van Laar HH. Modelling Crop-weed Interactions: CABI Publishing, 1993

964 Lamb A, Green R, Bateman I, Broadmeadow M, Bruce T, Burney J, et al. The potential for  
965 land sparing to offset greenhouse gas emissions from agriculture. Nature Climate  
966 Change 2016; 6: 488-492, <http://dx.doi.org/10.1038/nclimate2910>

967 Lark RM, Milne AE. Boundary line analysis of the effect of water-filled pore space on nitrous  
968 oxide emission from cores of arable soil. European Journal of Soil Science 2016; 67:  
969 148-159, <http://dx.doi.org/10.1111/ejss.12318>

970 Li KY, De Jong R, Boisvert JB. An exponential root-water-uptake model with water stress  
971 compensation. Journal of hydrology 2001, 252(1), 189-204.

972 Milne AE, Bell JR, Hutchison WD, van den Bosch F, Mitchell PD, Crowder D, et al. The Effect  
973 of Farmers' Decisions on Pest Control with Bt Crops: A Billion Dollar Game of  
974 Strategy. *Plos Computational Biology* 2015; 11,  
975 <http://dx.doi.org/10.1371/journal.pcbi.1004483>

976 Milne AE, Haskard KA, Webster CP, Truan IA, Goulding KWT, Lark RM. Wavelet analysis  
977 of the correlations between soil properties and potential nitrous oxide emission at farm  
978 and landscape scales. *European Journal of Soil Science* 2011; 62: 467-478,  
979 <http://dx.doi.org/10.1111/j.1365-2389.2011.01361.x>

980 Milne AE, Lark RM, Addiscott TM, Goulding KWT, Webster CP, O'Flaherty S. Wavelet  
981 analysis of the scale- and location-dependent correlation of modelled and measured  
982 nitrous oxide emissions from soil. *European Journal of Soil Science* 2005; 56: 3-17,  
983 <http://dx.doi.org/10.1111/j.1365-2389.2004.00650.x>

984 Monteith JL. Conservative behaviour in the response of crops to water and light. In: Rabbinge  
985 R, Goudriaan J, Van Keulen H, Penning de Vries FWT, Van Laar HH, editors.  
986 *Theoretical Production Ecology: Reflections and Prospects*. Pudoc, Wageningen, The  
987 Netherlands, 1990, pp. 3-16

988 Monteith JL, Moss CJ. Climate and the Efficiency of Crop Production in Britain [and  
989 Discussion]. *Philosophical Transactions of the Royal Society of London B: Biological*  
990 *Sciences* 1977; 281: 277-294, 10.1098/rstb.1977.0140

991 Nömmik H. Investigations on Denitrification in Soil. *Acta Agriculturae Scandinavica* 1956; 6:  
992 195-228, <http://dx.doi.org/10.1080/00015125609433269>

993 Orr RJ, Murray PJ, Eyles CJ, Blackwell MSA, Cardenas LM, Collins AL, et al. The North  
994 Wyke Farm Platform: effect of temperate grassland farming systems on soil moisture  
995 contents, runoff and associated water quality dynamics. *European Journal of Soil*  
996 *Science* 2016; 67: 374-385, <http://dx.doi.org/10.1111/ejss.12350>

997 Parton WJ, Holland EA, Del Grosso SJ, Hartman MD, Martin RE, Mosier AR, et al.  
998 Generalized model for NO<sub>x</sub> and N<sub>2</sub>O emissions from soils. Journal of Geophysical  
999 Research-Atmospheres 2001; 106: 17403-17419,  
1000 <http://dx.doi.org/10.1029/2001jd900101>

1001 Parton WJ, Schime DS, Ojima DS, Cole CV. A general model for soil organic matter dynamics:  
1002 sensitivity to litter chemistry, texture and management. In: Bryant RB, Arnold RW,  
1003 editors. Quantitative Modeling of Soil Forming Processes. SSSA Special Publication  
1004 39, Madison, WI, 1994, pp. 147-167

1005 Phalan B, Onial M, Balmford A, Green RE. Reconciling Food Production and Biodiversity  
1006 Conservation: Land Sharing and Land Sparing Compared. Science 2011; 333: 1289-  
1007 1291, <http://dx.doi.org/10.1126/science.1208742>

1008 Rawls WJ. Estimating Soil Bulk-Density from Particle-Size Analysis and Organic-Matter  
1009 Content. Soil Science Soil Science 1983; 135: 123-125

1010 Rolston DE, Rao PSC, Davidson JM, Jessup RE. Simulation of denitrification losses of nitrate  
1011 fertilizer applied to uncropped, cropped, and manure-amended field plots. Soil Science  
1012 1984; 137: 270-279, <http://dx.doi.org/10.1097/00010694-198404000-00009>

1013 Schapendonk A, Stol W, van Kraalingen DWG, Bouman BAM. LINGRA, a sink/source model  
1014 to simulate grassland productivity in Europe. European Journal of Agronomy 1998; 9:  
1015 87-100, [http://dx.doi.org/10.1016/s1161-0301\(98\)00027-6](http://dx.doi.org/10.1016/s1161-0301(98)00027-6)

1016 Semenov MA, Jamieson PD, Martre P. Deconvoluting nitrogen use efficiency in wheat: A  
1017 simulation study. European Journal of Agronomy 2007; 26: 283-294,  
1018 <http://dx.doi.org/10.1016/j.eja.2006.10.009>

1019 Semenov MA, Stratonovitch P. Adapting wheat ideotypes for climate change: accounting for  
1020 uncertainties in CMIP5 climate projections. Climate Research 2015; 65: 123-139,  
1021 <http://dx.doi.org/10.3354/cr01297>

- 1022 Senapati N, Chabbi A, Giostri AF, Yeluripati JB, Smith P. Modelling nitrous oxide emissions  
1023 from mown-grass and grain-cropping systems: Testing and sensitivity analysis of  
1024 DailyDayCent using high frequency measurements. *Science of the Total Environment*  
1025 2016; 572: 955-977, <http://dx.doi.org/10.1016/j.scitotenv.2016.07.226>
- 1026 Sharpley AN. Depth of Surface Soil-runoff Interaction as Affected by Rainfall, Soil Slope, and  
1027 Management1. *Soil Science Society of America Journal* 1985; 49: 1010-1015,  
1028 <http://dx.doi.org/10.2136/sssaj1985.03615995004900040044x>
- 1029 Sharps K, Masante D, Thomas A, Jackson B, Redhead J, May L, et al. Comparing strengths  
1030 and weaknesses of three ecosystem services modelling tools in a diverse UK river  
1031 catchment. *Science of the Total Environment* 2017; 584: 118-130,  
1032 [10.1016/j.scitotenv.2016.12.160](http://dx.doi.org/10.1016/j.scitotenv.2016.12.160)
- 1033 Shibu ME, Leffelaar PA, van Keulen H, Aggarwal PK. LINTUL3, a simulation model for  
1034 nitrogen-limited situations: Application to rice. *European Journal of Agronomy* 2010;  
1035 32: 255-271, [10.1016/j.eja.2010.01.003](http://dx.doi.org/10.1016/j.eja.2010.01.003)
- 1036 Smith P, Smith JU, Powelson DS, McGill WB, Arah JRM, Chertov OG, et al. A comparison of  
1037 the performance of nine soil organic matter models using datasets from seven long-term  
1038 experiments. *Geoderma* 1997; 81: 153-225
- 1039 Storkey J, Macdonald AJ, Poulton PR, Scott T, Kohler IH, Schnyder H, et al. Grassland  
1040 biodiversity bounces back from long-term nitrogen addition. *Nature* 2015; 528: 401-  
1041 404, <http://dx.doi.org/10.1038/nature16444>
- 1042 Storn R, Price K. Differential evolution - A simple and efficient heuristic for global  
1043 optimization over continuous spaces. *Journal of Global Optimization* 1997; 11: 341-  
1044 359, <http://dx.doi.org/10.1023/a:1008202821328>



1045 Tilman D, Fargione J, Wolff B, D'Antonio C, Dobson A, Howarth R, et al. Forecasting  
1046 agriculturally driven global environmental change. *Science* 2001; 292: 281-284,  
1047 <http://dx.doi.org/10.1126/science.1057544>

1048 van Genuchten MT. A closed-form equation for predicting the hydraulic conductivity of  
1049 unsaturated soils. *Soil Science Society of America Journal* 1980; 44: 892-898

1050 Van Ittersum MK, Leffelaar PA, Van Keulen H, Kropff MJ, Bastiaans L, Goudriaan J.  
1051 Developments in modelling crop growth, cropping systems and production systems in  
1052 the Wageningen school. *NJAS - Wageningen Journal of Life Sciences* 2003; 50: 239-  
1053 247, [http://dx.doi.org/10.1016/S1573-5214\(03\)80009-X](http://dx.doi.org/10.1016/S1573-5214(03)80009-X)

1054 van Laar HH, Goudriaan J, van Keulen H. SUCROS97: Simulation of crop growth for potential  
1055 and water-limited production situations as applied to spring wheat. *Quantitative*  
1056 *Approaches in Systems Analysis*. ab-dlo, Netherlands, 1997

1057 Watts CW, Clark LJ, Poulton PR, Powlson DS, Whitmore AP. The role of clay, organic carbon  
1058 and long-term management on mouldboard plough draught measured on the Broadbalk  
1059 wheat experiment at Rothamsted. *Soil Use and Management* 2006; 22: 334-341

1060 Whitehead PG, Jin L, Crossman J, Comber S, Johnes PJ, Daldorph P, et al. Distributed and  
1061 dynamic modelling of hydrology, phosphorus and ecology in the Hampshire Avon and  
1062 Blashford Lakes: Evaluating alternative strategies to meet WFD standards. *Science of*  
1063 *the Total Environment* 2014; 481: 157-166,  
1064 <http://dx.doi.org/10.1016/j.scitotenv.2014.02.007>

1065 Whitmore AP, Whalley WR, Bird NRA, Watts CW, Gregory AS. Estimating soil strength in  
1066 the rooting zone of wheat. *Plant and Soil* 2011; 339: 363-375,  
1067 <http://dx.doi.org/10.1007/s11104-010-0588-7>

1068 Wolf J. User guide for LINTUL4 and LINTUL4V: Simple generic model for simulation of  
1069 crop growth under potential, water limited and nitrogen limited conditions Wageningen  
1070 UR, Wageningen, 2012, pp. 58

1071 Wolf J, de Wit CT, Janssen BH, Lathwell DJ. Modelling long-term crop response to fertilizer  
1072 phosphorus. I. The model. *Agronomy Journal* 1987; 79: 445-451

1073 Wösten JHM, Lilly A, Nemes A, Le Bas C. Development and use of a database of hydraulic  
1074 properties of European soils. *Geoderma* 1999; 90: 169-185,  
1075 [http://dx.doi.org/10.1016/s0016-7061\(98\)00132-3](http://dx.doi.org/10.1016/s0016-7061(98)00132-3)

1076

1077

1078

1079

1080